ISSN: 2754-4915

Journal of Material Sciences & Manufacturing Research

SCIENTIFIC Research and Community

Research Article

Open Access

The Use of a Novel Graphitic Carbon Nitride/Cobalt Molybdate (G-C_3n_4/$ComoO_4$) Nanocomposites for the Doxycycline Removal by Photocatalytic Degradation in Pharmaceutical Industry Wastewaters and the Evaluation of Microtox (Aliivibrio Fischeri) and Daphnia Magna Acute Toxicity Assays

Rukiye Oztekin and Delia Teresa Sponza*

Engineering Faculty, Department of Environmental Engineering, Dokuz Eylul University, Tınaztepe Campus, Turkey

ABSTRACT

In this study, a novel graphitic carbon nitride/cobalt molybdate (g-C_3N_4/$CoMoO_4$) nanocomposites (NCs) as a photocatalys was examined during photocatalytic degradation process in the efficient removal of Doxycycline (DOX) from pharmaceutical industry wastewater plant, İzmir, Turkey. Different pH values (3.0, 4.0, 6.0, 7.0, 9.0 and 11.0), increasing DOX concentrations (5 mg/l, 15 mg/l, 30 mg/l and 45 mg/l), increasing g-C_3N_4/$CoMoO_4$ NCs concentrations (1 mg/l, 2 mg/l, 3 mg/l, 4 mg/l, 6 mg/l, 8 mg/l and 10 mg/l), different g-C_3N_4/$CoMoO_4$ NCs mass ratios (5/5, 6/4, 7/3, 8/2, 9/1, 1/9, 2/8, 3/7 and 4/6), increasing recycle times (1., 2., 3., 4., 5., 6. and 7.) was operated during photocatalytic degradation process in the efficient removal of DOX in pharmaceutical industry wastewater. The characteristics of the synthesized nanoparticles (NPs) were assessed using X-Ray Difraction (XRD), Field Emission Scanning Electron Microscopy (FESEM), Energy-Dispersive X-Ray (EDX), Fourier Transform Infrared Spectroscopy (FTIR), Transmission Electron Microscopy (TEM), and Diffuse reflectance UV-Vis spectra (DRS) analyses, respectively. The acute toxicity assays were operated with Microtox (*Aliivibrio fischeri* also called *Vibrio fischeri)* and *Daphnia magna* acute toxicity tests. ANOVA statistical analysis was used for all experimental samples. The maximum 99% DOX removal efficiency was obtained during photocatalytic degradation process in pharmaceutical industry wastewater, at 150 W UV-vis light irradiation power, after 180 min photocatalytic degradation time, at pH=9.0 and at 25°C, respectively. The maximum 99% DOX removal was found with photocatalytic degradation process in pharmaceutical industry wastewater, at 30 mg/l DOX, at 150 W UV-vis light irradiation power, after 180 min, at pH=9.0 and at 25°C, respectively. The maximum 99% DOX removal was measured to 8 mg/l g-C3N4/$CoMoO_4$ NCs with photocatalytic degradation process in pharmaceutical industry wastewater, at 30 mg/l DOX, at 150 W UV-vis light irradiation power, after 180 min, at pH=9.0 and at 25oC, respectively. The maximum 99% DOX removal was observed at 6/4wt g-C_3N_4/$CoMoO_4$ NCs mass ratios at 30 mg/l DOX, at 150 W UV-vis light irradiation power, after 180 min, at pH=9.0 and at 25°C, respectively. The maximum 99% DOX removal was obtained in pharmaceutical industry wastewater during photocatalytic degradation process, after 1. recycle time, at 30 mg/l DOX, 8 mg/l g-C_3N_4/$CoMoO_4$ NCs, at 6/4wt g-C_3N_4/$CoMoO_4$ NCs mass ratio, after 180 min, at pH=9.0 and at 25°C, respectively. 95.33% maximum Microtox (*Aliivibrio fischeri*) acute toxicity removal was found in DOX=30 mg/l after 180 min photocatalytic degradation time, and at 60°C, respectively. It was observed an inhibition effect of DOX=45 mg/l to Microtox with *Vibrio fischeri* after 180 min, and at 60°C. 91.27% maximum *Daphnia magna* acute toxicity removal was obtained in DOX=30 mg/l after 180 min and at 60°C, respectively. It was observed an inhibition effect of DOX=45 mg/l to *Daphnia magna* after 180 min, and at 60°C. DOX concentrations > 30 mg/l decreased the acute toxicity removals by hindering the photocatalytic degradation process. Similarly, a significant contribution of increasing DOX concentrations to acute toxicity removal at 60°C after 180 min, was not observed. It can be concluded that the toxicity originating from the DOX is not significant and the real acute toxicity throughout photocatalytic degradation process was attributed to the pharmaceutical industry wastewater, to their metabolites and to the photocatalytic degradation process by-products. As a result, the a novel g-C_3N_4/$CoMoO_4$ NCs photocatalyst during photocatalytic degradation process in pharmaceutical industry wastewater was stable in harsh environments such as acidic, alkaline, saline, and then was still effective process. When the amount of contaminant was increased, the a novel g-C_3N_4/$CoMoO_4$ NCs photocatalys during photocatalytic degradation process performance was still considerable. The synthesis and optimization of g-C_3N_4/$CoMoO_4$ heterostructure photocatalyst provides insights into the effects of preparation conditions on the material's characteristics and performance, as well as the application of the effectively designed photocatalyst in the removal of antibiotics, which can potentially be deployed for purifying wastewater, especially pharmaceutical wastewater. Finally, the combination of a simple, easy operation preparation process, excellent performance and cost effective, makes this a novel g-C_3N_4/$CoMoO_4$ NCs a promising option during photocatalytic degradation process in pharmaceutical industry wastewater treatment.

***Corresponding authors**

Delia Teresa Sponza, Engineering Faculty, Department of Environmental Engineering, Dokuz Eylül University, Tınaztepe Campus, Turkey.

Received: March 05, 2022; **Accepted:** March 15, 2023; **Published:** March 31, 2023

Keywords: ANOVA Statistical Analysis, Antibiotics, Coronavirus Disease-2019 (COVID-19), Diffuse Reflectance UV-Vis spectra (DRS), Doxycycline, Electrochemical Filtration Process, Energy-Dispersive X-ray (EDX), Field Emission Scanning Electron Microscopy (FESEM), Fourier Transform İnfrared Spectroscopy (FTIR), Microtox (*Aliivibrio fischeri* or *Vibrio fischeri*) and *Daphnia magna* Acute Toxicity Tests, Novel Graphitic Carbon Nitride/Cobalt Molybdate (g-C_3N_4/$CoMoO_4$) Nanocomposites, Pharmaceutical İndustry Wastewater, Transmission Electron Microscopy (TEM), X-ray Diffraction (XRD)

Introduction

Emerging contaminants (ECs), sometimes known as contaminants of emerging concern (CECs) can refer to a wide variety of artificial or naturally occurring chemicals or materials that are harmful to human health after long-term disclosure. ECs can be classified into several classes, including agricultural contaminants (pesticides and fertilizers), medicines and antidote drugs, industrial and consumer waste products, and personal care and household cleaning products [1,2]. Antibiotics are one of the ECs that have raised concerns in the previous two decades because they have been routinely and widely used in human and animal health care, resulting in widespread antibiotic residues discharged in surface, groundwater, and wastewater.

Antibiotics, which are widely utilized in medicine, poultry farming and food processing, have attracted considerable attention due to their abuse and their harmful effects on human health and the ecological environment [3-6]. The misuse of antibiotics induces Deoxyribonucleic Acid (DNA) contamination and accelerates the generation of drug-resistant bacteria and super-bacteria, thus, some diseases are more difficult to cure [7-10]. A number of studies have revealed that the level of antibiotics in the soil, air and surface water, and even in potable water, is excessive in many areas, which will ultimately accumulate in the human body via drinking water and then damage the body's nervous system, kidneys and blood system [11-13]. Therefore, it is necessary to develop an efficient method to remove antibiotics present in pharmaceutical industry wastewater.

The uncontrolled, ever-growing accumulation of antibiotics and their residues in the environment is an acute modern problem. Their presence in water and soil is a potential hazard to the environment, humans, and other living beings. Many therapeutic agents are not completely metabolized, which leads to the penetration of active drug molecules into the biological environment, the emergence of new contamination sources, the wide spread of bacteria and microorganisms with multidrug resistance [14-15]. Modern pharmaceutical wastewater facilities do not allow efficient removal of antibiotic residues from the environment, which leads to their accumulation in ecological systems [16-19]. Global studies of river pollution with antibiotics have shown that 65% of surveyed rivers in 72 countries on 6 continents are contaminated with antibiotics [20]. According to the World Health Organization (WHO), surface and groundwater, as well as partially treated water, containing antibiotics residue and other pharmaceuticals, typically at < 100 ng/l concentrations, whereas treated water has < 50 ng/l concentrations, respectively [21]. However, the discovery of ECs in numerous natural freshwater sources worldwide is growing yearly. Several antibiotic residues have been reported to have been traced at concentrations greater than their ecotoxicity endpoints in the marine environment, specifically in Europe and Africa [22]. Thus, the European Union's Water Framework Directive enumerated certain antibiotics as priority contaminants [23,24]. In some rivers, the concentrations were so high that they posed a real danger to both the ecosystem and human health. This matter, the development of effective approaches to the removal of antibiotics from the aquatic environment is of great importance.

The removal of antibiotics and their residues from water and wastewater prior to their final release into the environment is of particular concern [25]. Modern purification methods can be roughly divided into the following three categories depending on the purification mechanism: biological treatment, chemical degradation, and physical removal. Each of these methods has its own advantages and disadvantages [25-28]. For example, biological purification can remove most antibiotic residues, but the introduction of active organisms into the aquatic environment can upset the ecological balance. Various chemical approaches (ozonation, chlorination, and Fenton oxidation) cannot provide complete purification and, in some cases, lead to the death of beneficial microorganisms due to low selectivity. Photocatalysis is widely used in new environmental control strategies [29-31]. However, this method has a number of key disadvantages, such as insufficient use of visible light, rapid annihilation of photogenerated carriers, and incomplete mineralization, which greatly limits its application [25].

DOX, a tetracycline antibiotic, combined with other drugs, has been widely used to minimise Coronavirus Disease-2019 (COVID-19) induced inflammation in 2020 [32]. So, of a sudden, the demand and production of DOX have increased many folds. Due to the high consumptions, there are many chances that DOX will come in effluent treatment through the urinal of COVID-19 patients. DOX will also come in pharmaceutical industries wastewater, which are producing DOX. These compounds can enter water resources through various channels, including human waste and inefficient industrial wastewater treatment [33]. DOX is also used to treat chest, skin, and dental infections. DOX pharmaceutical compounds enter water resources in various ways, such as human and animal excretions and inefficient industrial wastewater treatment [33]. They also enter the environment due to the improper disposal of expired pharmaceuticals in the garbage or sewage system. The traditional methods for treating such wastewater like coagulation, flocculation, or precipitation lacks efficiency and cannot remove them completely [34-36]. On the other hand, biological treatments are time-consuming and produce a large quantity of sludge that cannot be used further [37]. However, most of these technologies have been reported to have drawbacks such as low efficiency, secondary pollution, and high capital costs. As a result, it is necessary to develop practical technologies based on modern world engineering science to find a better and more cost-effective solution to treat water and wastewater for human consumption. In recent years, advanced oxidation processes (AOPs) have piqued the interest of many researchers due to their potential application in the efficient mineralisation of refractory substances, more effective and sustainable in the long term [38-40].

Numerous materials have been reported to have the potential and capacity to treat water or wastewater polluted with these antibiotics residue by applying the processes of adsorption and catalytic oxidation during the last few decades. The reported materials include mesoporous carbon beads biochar, clay minerals, activated carbon, cellulose and chitos [41-53]. As a result of engineering and science evolution, and in complement to the urgent need to increase the adsorption capability of antibiotic contaminants, more advanced materials such as carbon nanotube (CnT), nano-zero valent iron (nZVI), nanoporous carbons, porous graphene and graphene oxide (GO), to date have been analyzed and improved in their ability to remove these ECs from water [2, 54-68].

Nanomaterials with a high specific surface area are a promising platform for the development and production of low-cost and highly efficient sorbents for various pollution molecules [69,70]. For example, graphene-based nanomaterials were utilized to remove antibiotics, which are adsorbed on the material surfaces due to π-π-, electrostatic or hydrophobic interactions, as well as the formation of hydrogen bonds [71-73]. Highly efficient antibiotic sorption was also observed when using highly porous, surface-active, and structurally stable silica-based materials, metal oxide NPs, and metal-organic frameworks [30,74-79]. The photocatalysts, which mainly rely on the production of highly oxidizing species such as hydroxyl radical ($OH^{\bullet}$) and superoxide anion radical ($O_2^{-\bullet}$), have been considered an effective approach for the degradation of antibiotics in water [80-83].

The two-dimensional (2D) g-C_3N_4 semiconductor has a wide range of applications in the environmental and energy fields because of its visible-light activity, unique physicochemical properties, excellent chemical stability and low-cost [84-85]. Some important limitations of the photocatalytic activity of g-C_3N_4 are its low specific surface area, fast recombination of electrons and holes and poor visible light absorption [86-88]. To improve the above problems, the construction of a heterojunction with a suitable band gap semiconductor (co-catalyst) has been shown to be a good strategy to improve the photocatalytic performance of g-C_3N_4, such as g-C_3N_4-based conventional type II heterostructures, g-C3N4-based Z-scheme heterostructures, and g-C_3N_4-based p–n heterostructures, etc. The unique "Z" shape as the transport pathway of photogenerated charge carriers in Z-scheme photocatalytic systems is the most similar system to mimic natural photosynthesis in the many g-C_3N_4-based heterojunction photocatalysts. The construction of Z-scheme photocatalytic systems can promote visible light utilization and carrier separation, and maintain the strong reducibility and oxidizability of semiconductors [89-93]. There are many studies on g-C_3N_4-based Z-scheme heterojunction photocatalysts, such as ZnO/g-C_3N_4, WO_3/g-C_3N_4, g-C_3N_4/ZnS, g-C_3N_4/$NiFe_2O_4$, g-C_3N_4/graphene/$NiFe_2O_4$, NiCo/ZnO/g-C_3N_4 and $Bi_2Zr_2O_7$/g-C_3N_4/Ag_3PO_4 respectively [86,87,94-102]. g-C_3N_4-based Z-scheme heterojunction photocatalysts have been made to improve the photocatalytic activity by combining with other semiconductor materials. Therefore, there are some problems with the single photocatalytic method, such as low adsorption ability, limited active sites and low removal efficiency. The integration of the adsorption and photocatalytic degradation of various organic pollutants is considered as a suitable and promising technology. On the other hand, it is still essential to fabricate photocatalysts with superior adsorption and degradation efficiencies.

g-C_3N_4 has been gaining great attention as a potential photocatalyst due to its stability and safety characteristics, as well as the fact that it can be facilely synthesized from low-cost raw materials. The low bandgap (~2.7 eV) can drive photo-oxidation reactions even under visible light [27,103,104]. However, the pure g-C_3N_4 has some drawbacks such as its low redox potential and high rate of recombination between photo-induced electrons and holes, which dramatically limits its photocatalytic efficiency. Several strategies have been investigated, including modification of the material's size and structure, nonmetal and metal doping and coupling with other photocatalysts. For example, Liu et al. improved bulk g-C_3N_4's performance in terms of Rhodamine B degradation from 30% to 100% by synthesizing mesoporous g-C_3N_4 nanorods through the nano-confined thermal condensation method. Dai et al. doped g-C_3N_4 with Cu through a thermal polymerization route and acquired a degradation rate of 90.5% with norfloxacin antibiotic. Synthesized hybridized g-C_3N_4/$ZnBi_2O_4$ for reduction of 4-nitrophenol and reached an optimal removal efficiency of 79%. Among all, the construction of heterostructure photocatalysts by coupling g-C_3N_4 with other semiconductors seems to be an effective strategy to prevent electron and hole recombination, hence improving photocatalytic efficiency for contaminant treatment [85,91,105-114].

$CoMoO_4$, a transition metal molybdate with narrow bandgap energy (2.1-2.8 eV), great redox activity, and strong catalytic electrochemical characteristics is also considered a promising visible-light-driven photocatalyst [115-117]. $CoMoO_4$ photocatalyst has been successfully applied for organic pollutant removal as well as bacterial inactivation (116,118-120]. Therefore, the application of $CoMoO_4$ for organic compound photodegradation is limited because of the low potential energy of the conduction band and fast recombination of photo-induced electrons and holes. Some studies have been conducted to address this issue. Umpathy and Neeraja investigated the photocatalytic activity of $CoMoO_4$ with 4-chlorophenol degradation by preparing $CoMoO_4$/TiO_2 nanocomposites (NCs), which showed higher efficiency 97.5% $CoMoO_4$/TiO_2 NCs as compared to that of 88% pure $CoMoO_4$. With their potential yet drawbacks to act as an individual photocatalyst, together with the compatibility in their bandgap energy, g-C_3N_4 and $CoMoO_4$ could be coupled to promisingly form a heterojunction displaying enhanced photocatalytic activity. The conduction band of g-C_3N_4 is more negative than that of $CoMoO_4$ (- 1.24 eV and 0.67 eV, respectively), while $CoMoO_4$ possesses a relatively positive valance band (2.63 eV) compared to the conduction band of g-C_3N_4, would theoretically facilitate the electron transition within the coupled photocatalyst to prolong the electron-hole separation [26]. In detail, under the illumination of visible light, both $CoMoO_4$ and g-C_3N_4 can be excited to generate electron-hole pairs. The photogenerated electrons in the conduction band of $CoMoO_4$ tend to transfer and recombine with the photogenerated holes in the valence band of g-C_3N_4. In this way, the larger number of photogenerated electrons accumulated in the conduction band of g-C_3N_4 can reduce the adsorbed O_2 to form more $O_2^{-\bullet}$. Meanwhile, the photogenerated holes left behind in the valence band of $CoMoO_4$ can oxidize the adsorbed H_2O to give $OH^{\bullet}$. However, the photocatalytic activity of the g-C_3N_4/$CoMoO_4$ system would be significantly increased, leading to the decomposition of organic compounds by $O_2^{-\bullet}$ and $OH^{\bullet}$ reactive species. Few studies have devised heterostructure photocatalyst with g-C_3N_4 and $CoMoO_4$. Habibi-Yangjeh et al. reported synthesizing visible-light-driven g-C_3N_4/Fe_3O_4/$CoMoO_4$ photocatalysts with removal efficiency over rhodamine B, methylene blue, and fuchsine of 62.9%, 72.8%, and 71.5%, respectively [121]. Zhang et al. further studied the photocatalytic ability of composite including g-C_3N_4 and a variation of $CoMoO_4$ ratio for methylene blue treatment, where the optimal composite showed to 94% degradation rate [122]. Therefore, in these previous works, influence factors on the synthesis of g-C_3N_4/$CoMoO_4$ have not been systematically studied.

In this study, a novel g-C_3N_4/$CoMoO_4$ NCs as a photocatalys was examined during photocatalytic degradation process in the efficient removal of DOX from pharmaceutical industry wastewater plant, İzmir, Turkey. Different pH values (3.0, 4.0, 6.0, 7.0, 9.0 and 11.0), increasing DOX concentrations (5 mg/l, 15 mg/l, 30 mg/l and 45 mg/l), increasing g-C_3N_4/$CoMoO_4$ NCs concentrations (1 mg/l, 2 mg/l, 3 mg/l, 4 mg/l, 6 mg/l, 8 mg/l and 10 mg/l), different g-C_3N_4/$CoMoO_4$ NCs mass ratios (5/5, 6/4, 7/3, 8/2, 9/1, 1/9, 2/8, 3/7 and 4/6), increasing recycle times (1., 2., 3., 4., 5., 6. and 7.) was operated during photocatalytic degradation process in the

efficient removal of DOX in pharmaceutical industry wastewater. The characteristics of the synthesized NPs were XRD, FESEM, EDX, FTIR, TEM and DRS analyses, respectively. The acute toxicity assays were operated with Microtox (Aliivibrio fischeri also called Vibrio fischeri) and Daphnia magna acute toxicity tests. ANOVA statistical analysis was used for all experimental samples.

Materıals and Methods

Characterization of Pharmaceutical Industry Wastewater

Characterization of the biological aerobic activated sludge proses from a pharmaceutical industry wastewater plant, İzmir, Turkey was performed. The results are given as the mean value of triplicate samplings (Table 1).

Table 1: Characterization of Pharmaceutical Industry Wastewater

Parameters	Unit	Concentrations
Chemical oxygen demand-total (COD_{total})	(mg/l)	4000
Chemical oxygen demand-dissolved ($COD_{dissolved}$)	(mg/l)	3200
Biological oxygen demand-5 days (BOD_5)	(mg/l)	1500
BOD_5 / $COD_{dissolved}$		0.5
Total organic carbons (TOC)	(mg/l)	1800
Dissolved organic carbons (DOC)	(mg/l)	1100
pH		8.3
Salinity as Electrical conductivity (EC)	(mS/cm)	1552
Total alkalinity as $CaCO_3$	(mg/l)	750
Total volatile acids (TVA)	(mg/l)	380
Turbidity (Nephelometric Turbidity unit, NTU)	NTU	7.2
Color	1/m	50
Total suspended solids (TSS)	(mg/l)	250
Volatile suspended solids (VSS)	(mg/l)	187
Total dissolved solids (TDS)	(mg/l)	825
Nitride (NO_2^-)	(mg/l)	1.7
Nitrate (NO_3^-)	(mg/l)	1.91
Ammonium (NH_4^+)	(mg/l)	2.3
Total Nitrogen (Total-N)	(mg/l)	3.2
SO_3^{-2}	(mg/l)	21.4
SO_4^{-2}	(mg/l)	29.3
Chloride (Cl^-)	(mg/l)	37.4
Bicarbonate (HCO_3^-)	(mg/l)	161
Phosphate (PO_4^{-3})	(mg/l)	16
Total Phosphorus (Total-P)	(mg/l)	40
Total Phenols	(mg/l)	70
Oil & Grease	(mg/l)	220
Cobalt (Co^{+3})	(mg/l)	0.2
Lead (Pb^{+2})	(mg/l)	0.4
Potassium (K^+)	(mg/l)	17
Iron (Fe^{+2})	(mg/l)	0.42
Chromium (Cr^{+2})	(mg/l)	0.44
Mercury (Hg^{+2})	(mg/l)	0.35
Zinc (Zn^{+2})	(mg/l)	0.11

Preparation of Graphitic Carbon Nitride (g-C_3N_4) Nanoparticles g-C_3N_4 was prepared by calcination of melamine ($C_3H_6N_6$) in a crucible with a lid at 550°C for 4 h. The obtained yellow powder was ground in an agate mortar after being cooled down to 25°C room temperature.

Preparation of Cobalt Molybdate ($CoMoO_4$) Nanoparticles

Intact $CoMoO_4$ was prepared cobalt nitrate [$Co(NO_3)_2$] and sodium molybdate (Na_2MoO_4) precursor was firstly dissolved in distilled water under the magnetic stirring condition for 30 min to obtain 1 M $Co(NO_3)_2$ and 1 M Na_2MoO_4 solutions, respectively. Then, the prepared $Co(NO_3)_2$ solution was slowly added to Na_2MoO_4 solution under a constant stirring condition for 1 h. After that, the obtained mixture was transferred into a stainless-steel autoclave for the hydrothermal process at 180°C for 6h.

Preparation of A Novel Graphitic Carbon Nitride/Cobalt Molybdate (g-C_3N_4/$CoMoO_4$) Nanocomposites

The g-C_3N_4/$CoMoO_4$ NCs was synthesized by the hydrothermal-calcination method. Firstly, 1 gram g-C_3N_4 NPs was added into distilled water and magnetically stirred for 30 min. The mixtures of $Co(NO_3)_2$ and Na_2MoO_4 were obtained by stirring certain amounts of these precursors in distilled water for 30 min. Then, the portions of prepared g-C_3N_4 were added to the mixtures to obtain the mass ratios of g-C_3N_4 to $CoMoO_4$ of 5/5, 6/4, 7/3, 8/2, 9/1, 1/9, 2/8, 3/7 and 4/6, respectively, and kept being stirred for another 1 h. The final mixtures were transferred into a 100 ml autoclave and reacted at 180°C for different hydrothermal (HT) times of 2 h, 4 h and 6 h. The final samples were centrifuged and washed with distilled water and ethanol (C_2H_6O) 2 times. Then, the samples were dried, and finally, the dried products were heated in a Muffle furnace at different calcination temperatures of 300°C, 400°C and 500°C for 4 h to get the target composites. The synthesis conditions and the corresponding sample names were summarized at Table 2.

Table 2: The Optimization Parameters of g-C_3N_4/$CoMoO_4$ NCs Samples

Sample Name	Mass Ratios of g-C_3N_4/ $CoMoO_4$ NCs	Calcination Temperature (°C) in 240 min	Hydrothermal Time (min) at 180°C
HT-2h-Cal300	8/2	300°C	120
HT-2h-Cal400	8/2	400°C	120
HT-2h-Cal500	8/2	500°C	120
HT-4h-Cal300	8/2	300°C	240
HT-4h-Cal400	8/2	400°C	240
HT-4h-Cal500	8/2	500°C	240
HT-6h-Cal300	8/2	300°C	360
HT-6h-Cal400	8/2	400°C	360
HT-6h-Cal500	8/2	500°C	360
5/5 wt, g-C_3N_4 / $CoMoO_4$	5/5	500°C	360
6/4 wt, g-C_3N_4 / $CoMoO_4$	6/4	500°C	360
7/3 wt, g-C_3N_4 / $CoMoO_4$	7/3	500°C	360

8/2 wt, g-C_3N_4 / $CoMoO_4$	8/2	500°C	360
9/1 wt, g-C_3N_4 / $CoMoO_4$	9/1	500°C	360
1/9 wt, g-C_3N_4 / $CoMoO_4$	1/9	500°C	360
2/8 wt, g-C_3N_4 / CoMoO4	2/8	500°C	360
3/7 wt, g-C_3N_4 / $CoMoO_4$	3/7	500°C	360
4/6 wt, g-C_3N_4 / $CoMoO_4$	4/6	500°C	360

Photocatalytic Degradation Reactor

A 2 liter cylinder quartz glass reactor was used for the photodegradation experiments in the pharmaceutical industry wastewater at different operational conditions. 1000 ml pharmaceutical industry wastewater was filled for experimental studies and the photocatalyst were added to the cylinder quartz glass reactors. The UV-A lamps were placed to the outside of the photo-reactor with a distance of 3 mm. The photocatalytic reactor was operated with constant stirring (1.5 rpm) during the photocatalytic degradation process. 10 ml of the reacting solution were sampled and centrifugated (at 10000 rpm) at different time intervals. The UV irradiation treatments were created using one or three UV-A lamp emitting in the 350–400 nm range (λmax = 368 nm, FWHM = 17 nm, Actinic BL TL-D 18W, Philips). Three 50 W UV-A lamps (Total: 150 W UV-A lamps) were used during experimental conditions for this study.

Characterization

X-Ray Diffraction Analysis

Powder XRD patterns were recorded on a Shimadzu XRD-7000, Japan diffractometer using Cu Kα radiation (λ = 1.5418 Å, 40 kV, 40 mA) at a scanning speed of 1° /min in the 10-80° 2θ range. Raman spectrum was collected with a Horiba Jobin Yvon-Labram HR UV-Visible NIR (200-1600 nm) Raman microscope spectrometer, using a laser with the wavelength of 512 nm. The spectrum was collected from 10 scans at a resolution of 2 /cm. The zeta potential was measured with a SurPASS Electrokinetic Analyzer (Austria) with a clamping cell at 300 mbar.

Field Emission Scanning Electron Microscopy (FESEM) and Energy Dispersive X-Ray (EDX) Spectroscopy Analysis

The morphological features and structure of the synthesized catalyst were investigated by FESEM (FESEM, Hitachi S-4700), equipped with an EDX spectrometry device (TESCAN Co., Model III MIRA) to investigate the composition of the elements present in the synthesized catalyst.

Fourier Transform Infrared Spectroscopy (FTIR) Analysis

The FTIR spectra of samples was recorded using the FT-NIR spectroscope (RAYLEIGH, WQF-510).

Transmission Electron Microscopy (TEM) Analysis

The structure of the samples were analysed TEM analysis. TEM analysis was recorded in a JEOL JEM 2100F, Japan under 200 kV accelerating voltage. Samples were prepared by applying one drop of the suspended material in ethanol onto a carbon-coated copper TEM grid, and allowing them to dry at 25°C room temperature.

Diffuse Reflectance UV-Vis Spectra (DRS) Analysis

DRS Analysis in the range of 200–800 nm were recorded on a Cary 5000 UV-Vis Spectrophotometer from Varian. DRS was used to monitor the CIP antibiotic concentration in experimental samples.

Analytical Procedures

Chemical oxygen demand-total (COD_{total}), chemical oxygen demand-dissolved ($COD_{dissolved}$), total phosphorus (Total-P), phosphate phosphorus (PO_4^{-3}-P), total nitrogen (Total-N), ammonium nitrogen (NH_4^+-N), nitrate nitrogen (NO_3^--N), nitrite nitrogen (NO_2^--N), biological oxygen demand 5-days (BOD_5), pH, Temperature [(°C)], total suspended solids (TSS), total volatile suspended solids (TVSS), total organic carbon (TOC), Oil, Chloride (Cl^-), total phenol, total volatile acids (TVA), disolved organic carbon (DOC), total alkalinity, turbidity, total dissolved solid (TDS), color, sulfide (SO_3^{-2}), sulfate (SO_4^{-2}), bicarbonate (HCO_3^-), salinity, cobalt (Co^{+3}), lead (Pb^{+2}), potassium (K^+), iron (Fe^{+2}), chromium (Cr^{+2}), Mercury (Hg^{+2}) and zinc (Zn^{+2}) were measured according to the Standard Methods (2017) 5220B, 5220D, 4500-P, 4500-PO_4^{-3}, 4500-N, 4500-NH_4^+, 4500-NO_3^-, 4500-NO_2^-, 5210B, 4500-H^+, 2320, 2540D, 2540E, 5310, 5520, 4500-Cl^-, 5530, 5560B, 5310B, 2320, 2130, 2540E, 2120, 4500-SO_3^{-2}, 4500-SO_4^{-2}, 5320, 2520, 3500-Co^{+3}, 3500-Pb^{+2}, 3500- K^+, 3500-Fe^{+2}, 3500-Cr^{+2}, 3500- Hg^{+2}, 3500-Zn^{+2}, respectively [122].

Total-N, NH_4^+-N, NO_3^--N, NO_2^--N, Total-P, PO_4^{-3}-P, total phenol, Co^{+3}, Pb^{+2}, K^+, Fe^{+2}, Cr^{+2}, Hg^{+2}, Zn^{+2}, SO_3^{-2}, and SO_4^{-2} were measured with cell test spectroquant kits (Merck, Germany) at a spectroquant NOVA 60 spectrophotometer.

The measurement of color was carried out following the methods described by Olthof and Eckenfelder and Eckenfelder [123,124]. According these methods, the color content was determined by measuring the absorbance at three wavelengths (445 nm, 540 nm and 660 nm), and taking the sum of the absorbances at these wavelengths. In order to identify the color in pharmaceutical industry wastewater (25 ml) was acidified at pH=2.0 with a few drops of 6 N HCl and extracted three times with 25 ml of ethyl acetate. The pooled organic phases were dehydrated on sodium sulphate, filtered and dried under vacuum. The residue was sylilated with bis(trimethylsylil)trifluoroacetamide (BSTFA) in dimethylformamide and analyzed by gas chromatography–mass spectrometry (GC-MS) and gas chromatograph (GC) (Agilent Technology model 6890N) equipped with a mass selective detector (Agilent 5973 inert MSD). Mass spectra were recorded using a VGTS 250 spectrometer equipped with a capillary SE 52 column (HP5-MS 30 m, 0.25 mm ID, 0.25 μm) at 220°C with an isothermal program for 10 min. The initial oven temperature was kept at 50°C for 1 min, then raised to 220°C at 25°C/min and from 200 to 300°C at 8°C/min, and was then maintained for 5.5 min. High purity He (g) was used as the carrier gas at constant flow mode (1.5 ml/min, 45 cm/s linear velocity).

The total phenol was monitored as follows: 40 ml of pharmaceutical industry wastewater was acidified to pH=2.0 by the addition of concentrated HCl. Total phenol was then extracted with ethyl acetate. The organic phase was concentrated at 40°C to about 1 ml and silylized by the addition of N,O-bis(trimethylsilyl) acetamide (BSA). The resulting trimethylsilyl derivatives were analysed by GC-MS (Hewlett-Packard 6980/HP5973MSD).

Methyl tertiary butyl ether (MTBE) was used to extract oil from the water and NPs. GC-MS analysis was performed on an Agilent gas chromatography (GC) system. Oil concentration was measured using a UV–vis spectroscopy fluorescence spectroscopy and a GC–MS (Hewlett-Packard 6980/HP5973MSD). UV–vis

absorbance was measured on a UV–vis spectrophotometer and oil concentration was calculated using a calibration plot which was obtained with known oil concentration samples.

Acute Toxicity Assays

Microtox Acute Toxicity Test

Toxicity to the bioluminescent organism *Aliivibrio fischeri* (also called *Vibrio fischeri* or *V. fischeri*) was assayed using the Microtox measuring system according to DIN 38412L34, L341, (EPS 1/RM/24 1992). Microtox testing was performed according to the standard procedure recommended by the manufacturer [125]. A specific strain of the marine bacterium, *V. fischeri*-Microtox LCK 491 kit was used for the Microtox acute toxicity assay. Dr. LANGE LUMIX-mini type luminometer was used for the microtox toxicity assay [126].

Daphnia magna Acute Toxicity Test

To test toxicity, 24-h born *Daphnia magna* were used as described in Standard Methods sections 8711A, 8711B, 8711C, 8711D and 8711E, respectively [127]. After preparing the test solution, experiments were carried out using 5 or 10 *Daphnia magna* introduced into the test vessels. These vessels had 100 ml of effective volume at 7.0– 8.0 pH, providing a minimum dissolved oxygen (DO) concentration of 6 mg/l at an ambient temperature of 20–25°C. Young Daphnia magna were used in the test (≤24 h old), 24–48 h exposure is generally accepted as standard for a *Daphnia magna* acute toxicity test. The results were expressed as mortality percentage of the *Daphnia magna*. Immobile animals were reported as dead *Daphnia magna*.

Statistical Analysis

ANOVA analysis of variance between experimental data was performed to detect F and P values. The ANOVA test was used to test the differences between dependent and independent groups [128]. Comparison between the actual variation of the experimental data averages and standard deviation is expressed in terms of F ratio. F is equal (found variation of the date averages/expected variation of the date averages). P reports the significance level, and d.f indicates the number of degrees of freedom. Regression analysis was applied to the experimental data in order to determine the regression coefficient R^2 [129]. The aforementioned test was performed using Microsoft Excel Program.

All experiments were carried out three times and the results are given as the means of triplicate samplings. The data relevant to the individual pollutant parameters are given as the mean with standard deviation (SD) values.

Results and Dıscussıons

A Novel g-C_3N_4/$CoMoO_4$ Nanocomposites Characteristics

The Results of X-Ray Diffraction (XRD) Analysis

The results of XRD analysis was observed to pure g-C_3N_4 NPs, pure $CoMoO_4$ NPs and g-C_3N_4/$CoMoO_4$ NCs, respectively, in pharmaceutical industry wastewater with photocatalytic degradation process for DOX antibiotic removal (Figure 1). The characterization peaks were observed at 2θ values of 13.11o, 24.56o and 28.34°, respectively, implying pure g-C_3N_4 NPs in pharmaceutical industry wastewater with photocatalytic degradation process for DOX antibiotic removal (Figure 1a). The characterization peaks were obtained at 2θ values of 19.20°, 26.44°, 28.41°, 39.62°, 49.27°, 58.89° and 65.27°, respectively, implying pure $CoMoO_4$ NPs in pharmaceutical industry wastewater with photocatalytic degradation process for DOX antibiotic removal (Figure 1b). The characterization peaks were found at 2θ values of 13.40°, 24.62°, 27.78°, 28.15°, 28.29°, 30.16°, 34.17°, 40.38°, 49.53°, and 57.64°, respectively, implying g-C_3N_4/$CoMoO_4$ NCs in pharmaceutical industry wastewater with photocatalytic degradation process for DOX antibiotic removal (Figure 1c).

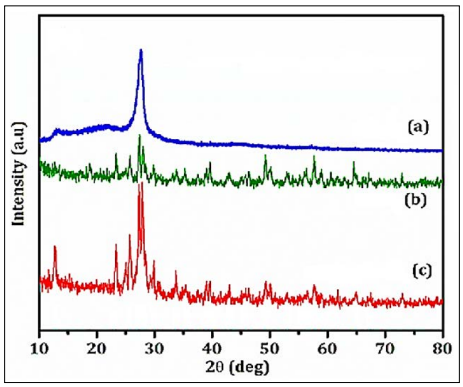

Figure 1: The XRD patterns of (a) pure g-C_3N_4 NPs (blue pattern), (b) pure $CoMoO_4$ NPs (green pattern) and (c) g-C_3N_4/$CoMoO_4$ NCs (red pattern), respectively, in pharmaceutical industry wastewater with photocatalytic degradation process for DOX antibiotic removal.

The Results of Diffuse Reflectance UV-Vis Spectra (DRS) Analysis

The absorption spectra of DOX was observed in DRS Analysis (Figure 2). First, the absorption spectra of DOX were obtained at a maximum concentration of 45 mg/l in the wavelength range from 250 nm to 750 nm using diffuse reflectance UV-Vis spectra (Figure 2). Absorption peaks were observed at wavelengths of 375 nm for pure g-C_3N_4 NPs (black pattern) (Figure 2a), 450 nm for pure $CoMoO_4$ NPs (red pattern) (Figure 2b), and 430 nm for g-C_3N_4/$CoMoO_4$ NCs (blue pattern) (Figure 2c), respectively, in pharmaceutical industry wastewater with photocatalytic degradation process for DOX antibiotic removal.

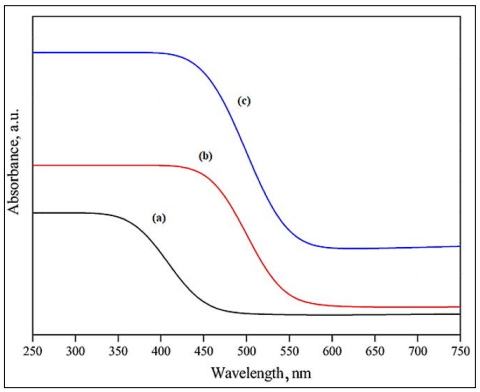

Figure 2: The DRS patterns of (a) pure g-C_3N_4 NPs (black pattern) (b) pure $CoMoO_4$ NPs (red pattern) and (c) g-C_3N_4/$CoMoO_4$ NCs (blue pattern), respectively, in pharmaceutical industry wastewater with photocatalytic degradation process for DOX antibiotic removal.

The Results of Field Emission Scanning Electron Microscopy (FESEM) Analysis

The morphological features of pure g-C_3N_4 NPs, pure $CoMoO_4$ NPs and g-C_3N_4/$CoMoO_4$ NCs were characterized through FE-SEM images (Figure 3). The FESEM images of pure g-C_3N_4 NPs were obtained in in pharmaceutical industry wastewater with photocatalytic degradation process for DOX antibiotic removal (Figure 3a). The FESEM images of pure $CoMoO_4$ NPs were observed in pharmaceutical industry wastewater with photocatalytic degradation process for DOX antibiotic removal (Figure 3b). The FESEM images of g-C_3N_4/$CoMoO_4$ NCs were characterized in pharmaceutical industry wastewater with photocatalytic degradation process for DOX antibiotic removal (Figure 3c).

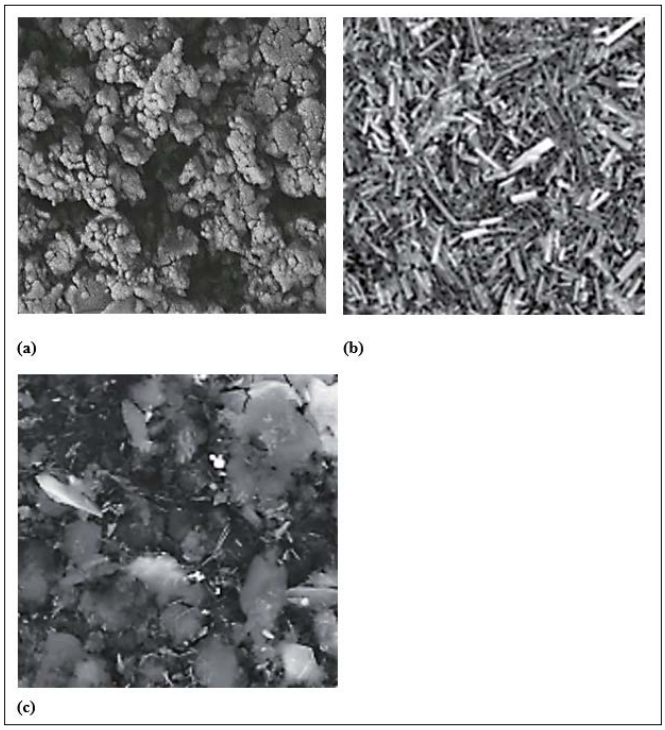

Figure 3: FESEM images of (a) pure g-C_3N_4 NPs, (b) pure $CoMoO_4$ NPs and (c) g-C_3N_4/$CoMoO_4$ NCs, respectively, in pharmaceutical industry wastewater with photocatalytic degradation process for DOX antibiotic removal.

The Results of Energy Dispersive X-Ray (EDX) Spectroscopy Analysis

The EDX analysis was also performed to investigate the composition of pure g-C_3N_4 NPs (Figure 4a), pure $CoMoO_4$ NPs (Figure 4b) and g-C_3N_4/$CoMoO_4$ NCs (Figure 4c), respectively, in pharmaceutical industry wastewater with photocatalytic degradation process for DOX antibiotic removal.

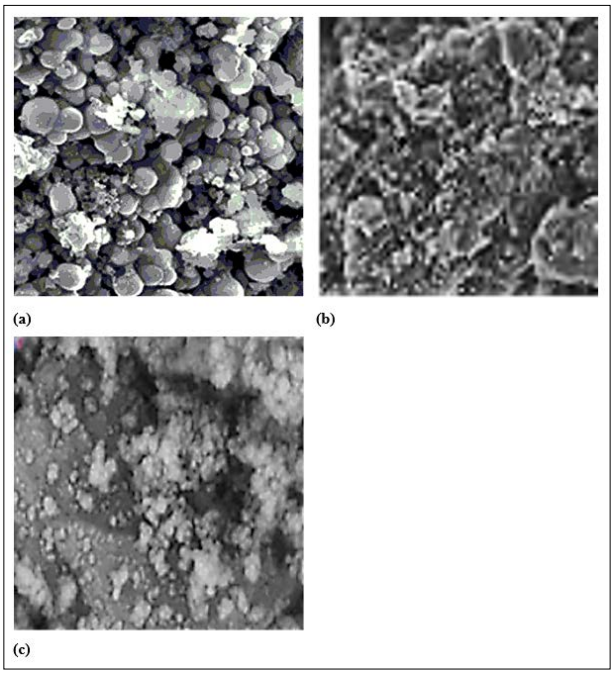

Figure 4: EDX spectrum of (a) pure g-C_3N_4 NPs, (b) pure $CoMoO_4$ NPs and (c) g-C_3N_4/$CoMoO_4$ NCs, respectively, in pharmaceutical industry wastewater with photocatalytic degradation process for DOX antibiotic removal.

The Results of Fourier Transform Infrared Spectroscopy (FTIR) Analysis

The FTIR spectrum of pure g-C_3N_4 NPs (blue spectrum), pure $CoMoO_4$ NPs (green spectrum) and g-C_3N_4/$CoMoO_4$ NCs (red spectrum), respectively, in pharmaceutical industry wastewater with photocatalytic degradation process for DOX antibiotic removal (Figure 5). The main peaks of FTIR spectrum for pure g-C_3N_4 NPs (blue spectrum) was observed at 805 1/cm, 1280 1/cm and 1956 1/cm wavenumber, respectively (Figure 5a). The main peaks of FTIR spectrum for pure $CoMoO_4$ NPs (green spectrum) was obtained at 912 1/cm, 1053 1/cm and 1450 1/cm wavenumber, respectively (Figure 5b). The main peaks of FTIR spectrum for g-C_3N_4/$CoMoO_4$ NCs (red spectrum) was determined at 560 1/cm, 820 1/cm, 1422 1/cm and 1997 1/cm wavenumber, respectively (Figure 5c).

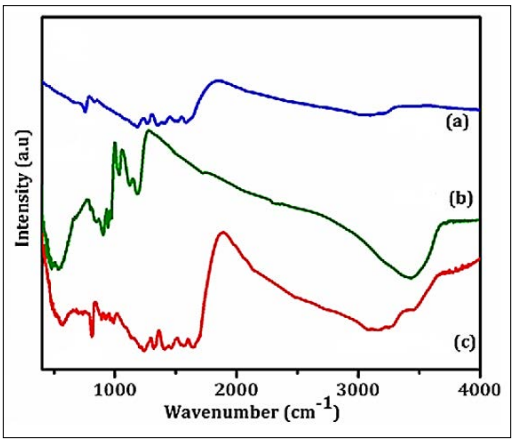

Figure 5: FTIR spectrum of (a) pure g-C_3N_4 NPs (blue spectrum), (b) pure $CoMoO_4$ NPs (green spectrum) and (c) g-C_3N_4/$CoMoO_4$ NCs (red spectrum), respectively, in pharmaceutical industry wastewater with photocatalytic degradation process for DOX antibiotic removal.

The Results of Transmission Electron Microscopy (TEM) Analysis

The TEM images of g-C_3N_4/$CoMoO_4$ NCs was observed in micromorphological structure level in pharmaceutical industry wastewater with photocatalytic degradation process for DOX antibiotic removal (Figure 6).

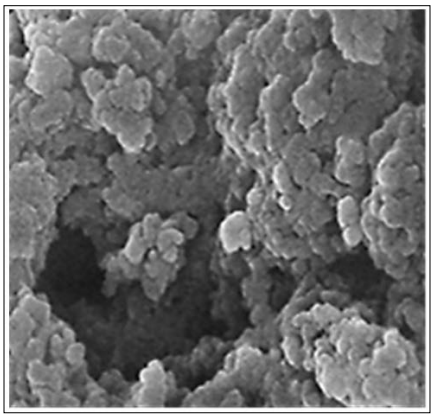

Figure 6: TEM images of g-C_3N_4/$CoMoO_4$ NCs in micromorphological structure level in pharmaceutical industry wastewater with photocatalytic degradation process for DOX antibiotic removal.

Effect of Increasing pH values for DOX Removal in Pharmaceutical Industry Wastewater during Photocatalytic Degradation Process

Increasing pH values (pH=3.0, pH=4.0, pH=6.0, pH=7.0, pH=9.0 and pH=11.0, respectively) was examined during photocatalytic degradation process in pharmaceutical industry wastewater for DOX removal (Figure 7). 44%, 56%, 67%, 85% and 96% DOX removal efficiencies was measured at pH=3.0, pH=4.0, pH=6.0, pH=7.0 and pH=11.0, respectively, at 150 W UV-vis light irradiation power, after 180 min photocatalytic degradation time, at 25°C (Figure 7). The maximum 99% DOX removal efficiency was obtained during photocatalytic degradation process in pharmaceutical industry wastewater, at 150 W UV-vis light irradiation power, after 180 min photocatalytic degradation time, at pH=9.0 and at 25°C, respectively (Figure 7).

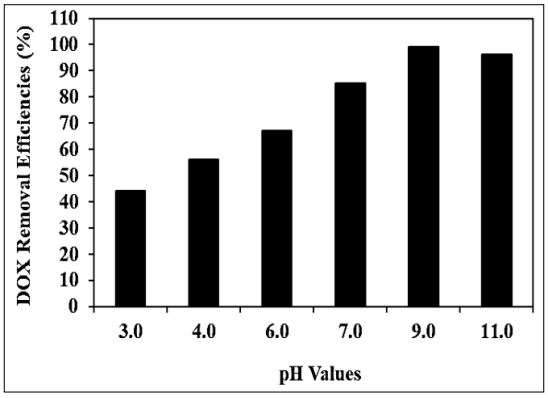

Figure 7: Effect of increasing pH values for DOX removal in pharmaceutical industry wastewater during photocatalytic degradation process, at 150 W UV-vis light irradiation power, after 180 min photocatalytic degradation time, at pH=9.0 and at 25°C, respectively.

Effect of Increasing DOX Concentrations for DOX Removal in Pharmaceutical Industry Wastewater during Photocatalytic Degradation Process

Increasing DOX concentrations (5 mg/l, 15 mg/l, 30 mg/l and 45 mg/l) were operated at 50 W sun light irradiation power, after 180 min photocatalytic degradation time, at pH=9.0, at 25°C, respectively (Figure 8). 85%, 94% and 77% DOX removal efficiencies were obtained to 5 mg/l, 15 mg/l and 45 mg/l DOX concentrations, respectively, at pH=9.0 and at 25°C (Figure 8). The maximum 99% DOX removal efficieny was found with photocatalytic degradation process in pharmaceutical industry wastewater, at 30 mg/l DOX, at 150 W UV-vis light irradiation power, after 180 min photocatalytic degradation time, at pH=9.0 and at 25°C, respectively (Figure 8).

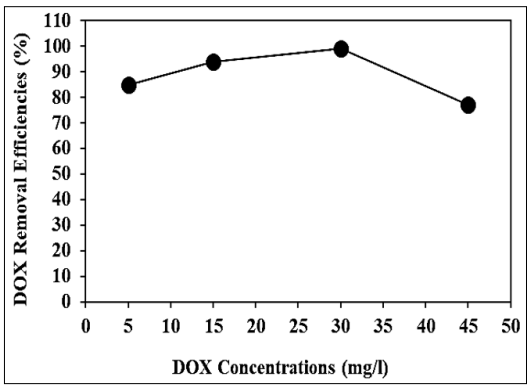

Figure 8: Effect of increasing DOX concentrations for DOX removal in pharmaceutical industry wastewater during photocatalytic degradation process, at 150 W UV-vis light irradiation power, after 180 min photocatalytic degradation time, at pH=9.0 and at 25°C, respectively.

Effect of Increasing g-C_3N_4/$CoMoO_4$ NCs Concentrations for DOX Removals in Pharmaceutical Industry Wastewater during Photocatalytic Degradation Process

Increasing g-C_3N_4/$CoMoO_4$ NCs concentrations (1 mg/l, 2 mg/l, 4 mg/l, 6 mg/l, 8 mg/l and 10 mg/l) were operated at 30 mg/l DOX, at 150 W UV-vis light irradiation power, after 180 min photocatalytic degradation time, at pH=9.0, at 25°C, respectively (Figure 9). 55%, 69%, 74%, 86% and 91% DOX removal efficiencies were obtained to 1 mg/l, 2 mg/l, 4 mg/l, 6 mg/l and 10 mg/l g-C_3N_4/$CoMoO_4$ NCs concentrations, respectively, at 15 mg/l DOX, at 150 W UV-vis light irradiation power, after 180 min photocatalytic degradation time, at pH=9.0, at 25°C, respectively (Figure 9). The maximum 99% DOX removal efficieny was measured to 8 mg/l g-C_3N_4/$CoMoO_4$ NCs with photocatalytic degradation process in pharmaceutical industry wastewater, at 30 mg/l DOX, at 150 W UV-vis light irradiation power, after 180 min photocatalytic degradation time, at pH=9.0 and at 25°C, respectively (Figure 9).

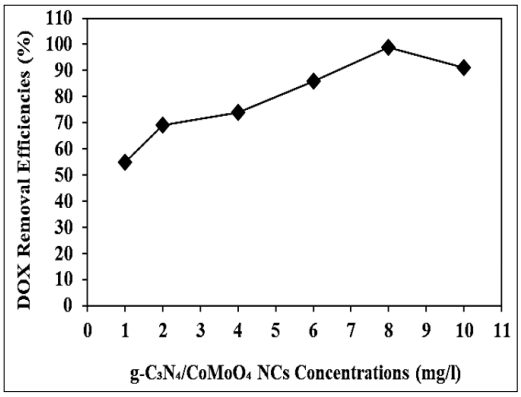

Figure 9: Effect of increasing g-C3N4/CoMoO4 NCs concentrations for DOX removal in pharmaceutical industry wastewater during photocatalytic degradation process, at 30 mg/l DOX, at 150 W UV-vis light irradiation power, after 180 min photocatalytic degradation time, at pH=9.0 and at 25°C, respectively.

Effect of Different g-C_3N_4/$CoMoO_4$ NCs Mass Ratios for DOX Removals in Pharmaceutical Industry Wastewater during Photocatalytic Degradation Process

Different g-C_3N_4/$CoMoO_4$ mass ratios (5/5wt, 6/4wt, 7/3wt, 8/2wt, 9/1wt, 1/9wt, 2/8wt, 3/7wt and 4/6wt, respectively) were examined for DOX removal in pharmaceutical industry wastewater during photocatalytic degradation process, at 30 mg/l DOX, at 150 W UV-vis light irradiation power, after 180 min photocatalytic degradation time, at pH=9.0 and at 25oC, respectively (Figure 10). 80%, 84%, 77%, 62%, 48%, 55%, 64% and 79% DOX removal efficiencies were measured at 5/5wt, 7/3wt, 8/2wt, 9/1wt, 1/9wt, 2/8wt, 3/7wt and 4/6wt g-C_3N_4/$CoMoO_4$ NCs mass ratios, respectively, at 30 mg/l DOX after 180 min photocatalytic degradation time, at pH=9.0 and at 25°C, respectively (Figure 10). The maximum 99% DOX removal efficiency was measured at 6/4wt g-C_3N_4/$CoMoO_4$ NCs mass ratios at 30 mg/l DOX, at 150 W UV-vis light irradiation power, after 180 min photocatalytic degradation time, at pH=9.0 and at 25°C, respectively (Figure 10).

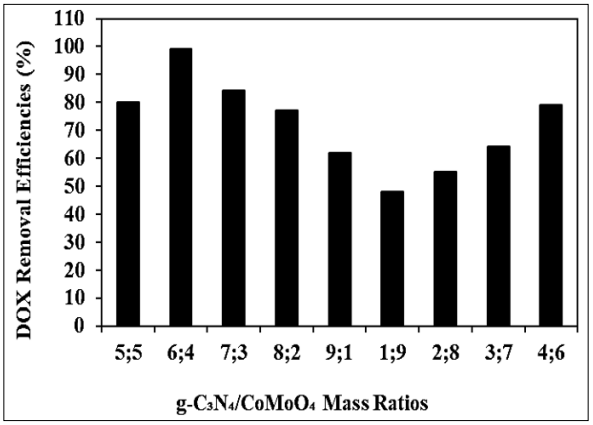

Figure 10: Effect of different g-C3N4/CoMoO4 NCs mass ratios for DOX removal in pharmaceutical industry wastewater during photocatalytic degradation process, at 30 mg/l DOX, at 150 W UV-vis light irradiation power, after 180 min photocatalytic degradation time, at pH=9.0 and at 25oC, respectively.

Effect of Different Recycle Times for DOX Removals in Pharmaceutical Industry Wastewater during Photocatalytic Degradation Process

Different recycle times (1., 2., 3., 4., 5., 6. and 7.) were operated for DOX removals in pharmaceutical industry wastewater during photocatalytic degradation process, at 30 mg/l DOX, 8 mg/l g-C_3N_4/$CoMoO_4$ NCs, at 6/4wt g-C_3N_4/$CoMoO_4$ NCs mass ratio, after 180 min photocatalytic degradation time, at pH=9.0 and at 25°C, respectively (Figure 11). 96%, 90%, 85%, 81%, 78% and 73% DOX removal efficiencies were measured after 2. recycle time, 3. recycle time, 4. recycle time, 5. recycle time, 6. recycle time and 7. recycle time, respectively, at 30 mg/l DOX, 8 mg/l g-C_3N_4/$CoMoO_4$ NCs, at 6/4wt g-C_3N_4/$CoMoO_4$ NCs mass ratio, after 180 min photocatalytic degradation time, at pH=9.0 and at 25°C, respectively (Figure 11). The maximum 99% DOX removal efficiency was measured in pharmaceutical industry wastewater during photocatalytic degradation process, after 1. recycle time, at 30 mg/l DOX, 8 mg/l g-C_3N_4/$CoMoO_4$ NCs, at 6/4wt g-C_3N_4/$CoMoO_4$ NCs mass ratio, after 180 min photocatalytic degradation time, at pH=9.0 and at 25°C, respectively (Figure 11).

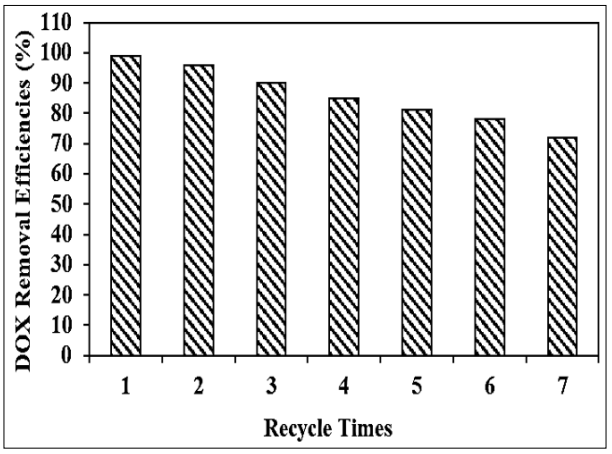

Figure 11: Effect of recycle times for DOX removal in pharmaceutical industry wastewater during photocatalytic degradation process, at 30 mg/l DOX, 8 mg/l g-C_3N_4/$CoMoO_4$ NCs, at 6/4wt g-C_3N_4/$CoMoO_4$ NCs mass ratio, at 150 W UV-vis light irradiation power, after 180 min photocatalytic degradation time, at pH=9.0 and at 25°C, respectively

Acute Toxicity Assays

Effect of Increasing DOX Concentrations on the Microtox (Aliivibrio fischeri or *Vibrio fischeri*) Acute Toxicity Removal Efficiencies in Pharmaceutical Industry Wastewater at Increasing Photocatalytic Degradation Time and Temperature

In Microtox with *Aliivibrio fischeri* (also called Vibrio fischeri) acute toxicity test, the initial EC90 values at pH=7.0 was found as 825 mg/l at 25°C (Table 3: SET 1). After 60 min, 120 min and 180 min photocatalytic degradation time, the EC_{90} values decreased to EC_{56}=416 mg/l to EC_{21}=238 mg/l and to EC_{11}=167 mg/l in DOX=30 mg/l at 30°C (Table 3: SET 3). The Microtox (*Aliivibrio fischeri*) acute toxicity removal efficiencies were 39.78%, 78.67% and 89.78% after 60 min, 120 min and 180 min, respectively, in DOX=30 mg/l and at 30°C (Table 3: SET 3).

Table 3: Effect of increasing DOX concentrations on Microtox (*Aliivibrio fischeri*) acute toxicity in pharmaceutical industry wastewater after photocatalytic degradation process, at 30°C and at 60°C, respectively

No	Parameters	Microtox (Aliivibrio fischeri) Acute Toxicity Values, * EC (mg/l)							
		25°C							
		0. Min		60. min		120. min		180. min	
		*EC_{90}		*EC		*EC		*EC	
1	Raw ww, control	825		EC_{70}=510		EC_{60}=650		EC_{49}=638	
		30°C				60°C			
		0. min	60. min	120. min	180. min	0. min	60. min	120. min	180. min
		*EC_{90}	*EC	*EC	*EC	*EC_{90}	*EC	*EC	*EC
2	Raw ww, control	825	EC_{70}= 580	EC_{50}= 580	EC_{39}= 548	825	EC_{55}= 550	EC_{40}= 590	EC_{29}= 688
3	DOX=5 mg/l	825	EC_{61}= 424	EC_{26}= 243	EC_{16}= 170	825	EC_{56}= 421	EC_{21}= 268	EC_{11}= 152
	DOX=15 mg/l	825	EC_{61}= 423	EC_{26}= 241	EC_{16}= 169	825	EC_{56}= 416	EC_{21}= 234	EC_{11}= 163
	DOX=30 mg/l	825	EC_{56} =416	EC_{21}= 238	EC_{11}= 167	825	EC_{51}= 552	EC_{16}= 542	EC_{6}= 502
	DOX=45 mg/l	825	EC_{66}= 410	EC_{31}= 232	EC_{21}= 164	825	EC_{61}= 405	EC_{26}= 220	EC_{16}= 150
* EC values were calculated based on COD_{dis} (mg/l).									

The EC_{90} values decreased to EC_{51}, to EC_{16} and to EC_6 after 60 min, 120 min and 180 min, respectively, in DOX=30 mg/l, at 60°C (Table 3: SET 3). The EC_{50}, the EC_{16} and the EC_6 values were measured as 552 mg/l, 542 mg/l and 502 mg/l, respectively, in DOX=30 mg/l at 60°C. The toxicity removal efficiencies were 45.33%, 84.22% and 95.33% after 60 min, 120 min and 180 min, respectively, in DOX=30 mg/l, at 60°C (Table 3: SET 3). 95.33% maximum Microtox (Aliivibrio fischeri) acute toxicity removal yield was found in DOX=30 mg/l after 180 min and at 60°C (Table 3: SET 3).

The EC_{90} values decreased to EC_{61}=424 mg/l to EC_{26}=243 mg/l and to EC_{16}=170 mg/l after 60 min, 120 min and 180 min, respectively, in DOX=5 mg/l at 30°C (Table 3: SET 3). The EC_{90} values decreased to EC_{61}=423 mg/l to EC_{26}=241 mg/l and to EC_{16}=169 mg/l after 60 min, 120 min and 180 min, respectively, in DOX=15 mg/l at 30°C. The EC_{90} values decreased to EC_{66}=410 mg/l to EC_{31}=232 mg/l and to EC_{21}=164 mg/l after 60 min, 120 min and 180 min, respectively, in DOX=45 mg/l at 30°C. The Microtox (Aliivibrio fischeri or Vibrio fischeri) acute toxicity removals were 84.22%, 84.21% and 78.67% in 5 mg/l, 15 mg/l and 45 mg/l DOX, respectively, after 180 min, at 30°C. It was obtained an inhibition effect of DOX=45 mg/l to Vibrio fischeri after 180 min and at 30°C (Table 3: SET 3).

The EC_{90} values decreased to EC_{56}=421 mg/l to EC_{21}=268 mg/l and to EC_{11}=152 mg/l after 60 min, 120 min and 180 min, respectively, in DOX=5 mg/l at 60°C (Table 3: SET 3). The EC_{90} values decreased to EC_{56}=416 mg/l to EC_{21}=234 mg/l and to EC_{11}=163 mg/l after 60 min, 120 and 180 min, respectively, in DOX=15 mg/l at 60°C. The EC_{90} values decreased to EC_{61}=405 mg/l to EC_{26}=220 mg/l and to EC_{16}=150 mg/l after 60 min, 120 and 180 min, respectively, in DOX=45 mg/l at 60°C. The Microtox (Aliivibrio fischeri or Vibrio fischeri) acute toxicity removals were 89.78%, 89.75% and 84.22% in 5 mg/l, 15 mg/l and 45 mg/l DOX, respectively, after 180 min, at 60°C. It was observed an inhibition effect of DOX=45 mg/l to Microtox with Vibrio fischeri after 180 min, and at 60°C (Table 3: SET 3).

Effect of Increasing DOX Concentrations on the Daphnia magna Acute Toxicity Removal Efficiencies in Pharmaceutical Industry Wastewater at Increasing Photocatalytic Degradation Time and Temperature

The initial EC_{50} values were observed as 850 mg/l at 25°C (Table 4: SET 1). After 60 min, 120 and 180 min photocatalytic degradation time, the EC_{50} values decreased to EC_{30}=352 mg/l to EC_{16}=242 mg/l and to EC_{11}=92 mg/l in DOX=30 mg/l, at 30°C (Table 4: SET 3). The toxicity removal efficiencies were 41.88%, 71.79% and 81.57% after 60 min, 120 min and 180 min, respectively, in DOX=30 mg/l at 30°C (Table 4: SET 3).

Table 4: Effect of increasing DOX concentrations on Daphnia magna acute toxicity in pharmaceutical industry wastewater after photocatalytic degradation process, at 30°C and at 60°C

No	Parameters	Daphnia magna Acute Toxicity Values, * EC (mg/l)							
		25°C							
		0. min		60. min		120. min		180. min	
		*EC_{50}		*EC		*EC		*EC	
1	Raw ww, control	850		EC_{45}=625		EC_{40}=370		EC_{29}=153	
		30°C				60°C			
		0. min	60. min	120. min	180. min	0. min	60. min	120. min	180. min
		*EC_{50}	*EC	*EC	*EC	*EC_{50}	*EC	*EC	*EC
2	Raw ww, control	850	EC_{39}= 468	EC_{34}= 228	EC_{23}= 111	850	EC_{34}= 373	EC_{29}= 210	EC_{18}= 71
3	DOX=5 mg/l	850	EC_{31}= 452	EC_{21}= 147	EC_{16}= 262	850	EC_{31}= 132	EC_{16}= 427	EC_{11}= 342
	DOX=15 mg/l	850	EC_{36}= 452	EC_{21}= 177	EC_{16}= 102	850	EC_{31}= 427	EC_{16}= 142	EC_{6}= 92
	DOX=30 mg/l	850	EC_{31}= 352	EC_{16}= 242	EC_{11}= 92	850	EC_{26}= 152	EC_{11}= 62	EC_{6}= 377
	DOX=45 mg/l	850	EC_{41}= 302	EC_{26}= 172	EC_{21}= 54	850	EC_{36}= 252	EC_{21}= 112	EC_{16}= 13
* EC values were calculated based on COD_{dis} (mg/l).									

The EC_{50} values decreased to EC_{26} to EC_{11} and to EC_6 after 60 min, 120 min and 180 min, respectively, in DOX=30 mg/l at 60°C (Table 4: SET 3). The EC_{26}, the EC_{11} and the EC_6 values were measured as 152 mg/l, 62 mg/l and 377 mg/l, respectively, in DOX=30 mg/l at 60°C. The toxicity removal efficiencies were 51.86%, 81.54% and 91.27% after 60 min, 120 min and 180 min, respectively, in DOX=30 mg/l at 60°C (Table 4: SET 3). 91.27% maximum Daphnia magna acute toxicity removal was obtained in DOX=30 mg/l after 180 min and at 60°C, respectively (Table 4: SET 3).

The EC_{50} values decreased to EC_{36}=452 mg/l to EC_{21}=147 mg/l and to EC_{16}=262 mg/l after 60 min, 120 min and 180 min, respectively, in DOX=5 mg/l at 30°C (Table 4: SET 3). The EC_{50} values decreased to EC_{36}=452 mg/l to EC_{21}=177 mg/l and to EC_{16}=102 mg/l after 60 min, 120 min and 180 min, respectively, in DOX=15 mg/l and at 30°C. The EC_{50} values decreased to EC_{41}=302 mg/l to EC_{26}=172 mg/l and to EC_{21}=54 mg/l after 60 min, 120 min and 180 min, respectively, in DOX=45 mg/l and at 30°C. The Daphnia magna acute toxicity removals were 71.14%, 71.48% and 62.13% in 5 mg/l, 15 mg/l and 45 mg/l DOX, respectively, after 180 min and at 30°C. It was observed an inhibition effect of DOX=45 mg/l to Daphnia magna after 180 min and at 30°C (Table 4: SET 3).

The EC_{50} values decreased to EC_{31}=132 mg/l to EC_{16}=427 mg/l and to EC_{11}=342 mg/l after 60 min, 120 min and 180 min, respectively, in DOX=5 mg/l and at 60°C (Table 4: SET 3). The EC_{50} values decreased to EC_{31}=427 mg/l to EC_{16}=142 mg/l and to EC_6=92 mg/l after 60 min, 120 min and 180 min, respectively, in DOX=15 mg/l and at 60°C. The EC_{50} values decreased to EC_{36}=252 mg/l to EC_{21}=112 mg/l and to EC_{16}=12 mg/l after 60 min, 120 min and 180 min, respectively, in DOX=45 mg/l and at 60°C. The Daphnia magna acute toxicity removals were 81.98%, 91.57% and 72.03% in 5 mg/l, 15 mg/l and 45 mg/l DOX, respectively, after 180 min and at 60°C. It was observed an inhibition effect of DOX=45 mg/l to Daphnia magna after 180 min and at 60°C (Table 4: SET 3). Increasing the DOX concentrations from 5 mg/l to 45 mg/l did not have a positive effect on the decrease of EC_{50} values as shown in Table 4 at SET 3. DOX concentrations > 30 mg/l decreased the acute toxicity removals by hindering the photocatalytic degradation process. Similarly, a significant contribution of increasing DOX concentration to acute toxicity removal at 60°C after 180 min of photocatalytic degradation time was not observed. Low toxicity removals found at high DOX concentrations could be attributed to their detrimental effect on the *Daphnia magna* (Table 4: SET 3).

Direct Effects of DOX Concentrations on the Acute Toxicity of Microtox (*Aliivibrio fischeri* or *Vibrio fischeri*) and *Daphnia magna* without Pharmaceutical Industry Wastewater after Photocatalytic Degradation Process

The acute toxicity test was performed in the samples containing 5 mg/l, 15 mg/l, 30 mg/l and 45 mg/l DOX concentrations, at 25°C room temperature. In order to detect the direct responses of Microtox (*Aliivibrio fischeri* or *Vibrio fischeri*) and Daphnia magna to the increasing DOX concentrations the toxicity test were performed without pharmaceutical industry wastewater after photocatalytic degradation process, at 25°C room temperature. The initial EC values and the the EC_{50} values were measured in the samples containing increasing DOX concentrations after 180 min photocatalytic degradation time. Table 5 showed the responses of Microtox (*Aliivibrio fischeri* or *Vibrio fischeri*) and *Daphnia magna* to increasing DOX concentrations.

Table 5: The responses of Microtox (*Aliivibrio fischeri* or *Vibrio fischeri*) and Daphnia magna acute toxicity tests in addition of increasing DOX concentrations without phamaceutical industry wastewater during photocatalytic degradation process after 180 min photocatalytic degradation time, at 25°C room temperature

DOX Conc. (mg/l)	Microtox (*Aliivibrio fischeri* or *Vibrio fischeri*) Acute Toxicity Test			*Daphnia magna* Acute Toxicity Test		
	Initial Acute Toxicity EC50 Value (mg/l)	Inhibitions after 180 min photocatalytic degradation time	EC Values (mg/l)	Initial Acute Toxicity EC_{50} Value (mg/l)	Inhibitions after 180 min photocatalytic degradation time	EC Values (mg/l)
5	EC_9= 23	-	-	EC_9=38	-	-
15	EC_{14}= 78	2	EC_1= 2	EC_{19}=98	4	EC_2=4
30	EC_{19}= 148	4	EC_3= 5	EC_{29}=198	5	EC_5=10
45	EC_{24}= 218	6	EC_5= 8	EC_{39}=298	8	EC_7=14

The acute toxicity originating only from 5 mg/l, 15 mg/l, 30 mg/l and 45 mg/l DOX were found to be low (Table 5). 5 mg/l DOX did not exhibited toxicity to *Aliivibrio fischeri* (or *Vibrio fischeri*) and *Daphnia magna* before and after 180 min photocatalytic degradation time. The toxicity atributed to the 15 mg/l, 30 mg/l and 45 mg/l DOX were found to be low in the samples without pharmaceutical industry wastewater after photocatalytic degradation process for the test organisms mentioned above. The acute toxicity originated from the DOX decreased significantly to EC1, EC3 and EC5 after 180 min photocatalytic degradation time. Therefore, it can be concluded that the toxicity originating from the DOX is not significant and the real acute toxicity throughout photocatalytic degradation process was attributed to the pharmaceutical industry wastewater, to their metabolites and to the photocatalytic degradation by-products (Table 5).

The Comparison with other Scientific Studies in the Literature

Comparison of our study "The use of a novel graphitic carbon nitride/cobalt molybdate (g-C_3N_4/$CoMoO_4$) nanocomposites for the Doxycycline removal by photocatalytic degradation in pharmaceutical industry wastewaters and the evaluation of Microtox (*Aliivibrio fischeri*) and *Daphnia magna* acute toxicity assays" with other scientific studies in the literature is summaried at Table 6.

Table 6: Photocatalytic decomposition of DOX in the wastewater of some different experimental conditions

Materials	Experimental Conditions (for maximum removal efficiencies)	Experimental Results	References
α-Bi_2O_3/g-C_3N_4	[DOX]=10 mg/l, [Material]=500 mg/l, [H_2O_2]=10 mM, Unadjusted pH, Xe lamp (150 W).	79.1% DOX removal after 30 min	[130]
Polymer-ZnO composite	[DOX]=50 mg/l, [Material]=250 mg/l, pH=7.0, UV C lamp (30 W).	92.7% DOX removal after 360 min	[131]
C,S-doped TiO_2	[DOX]=6.5x10^{-5} M, [Material]=1000 mg/l, 26 W Delux UV lamp and 8 W Maxus visible light lamp.	Highest removal rate constant: k_{UV}=9.0x10^{-3} 1/min k_{Vis}= 7.7x10^{-3} 1/min	[132]
MWCNTs/α-Bi_2O_3	[DOX]=10 mg/l, [Material]=1000 mg/l, 150 W Xe lamp with a UV cut-off filter.	91% DOX removal after 120 min	[133]
BiOBr/$FeWO_4$	[Material]=1000 mg/l, 300 W Xenon lamp.	90.1% DOX after 60 min	[134]
P25-500	[DOX]=5 mg/l, [Material]=250 mg/l, Unadjusted pH, UVA lamp.	81.29% DOX after 120 min	[135]
g-C_3N_4/$CoMoO_4$	[DOX]=30 mg/l, [Material]=1000 mg/l, pH=9.0, wt/wt g-C_3N_4/$CoMoO_4$ mass ratio=6/4, Three 50 W UV-A lamps emitting in the 350–400 nm range (λmax = 368 nm, FWHM = 17 nm, Actinic BL TL-D 18W, Philips), Recycle time= 7 times, Reusability Acute toxicity assays= Microtox (*Aliivibrio fischeri*) and *Daphnia magna* acute toxicity tests, Statistical analysis and Cost evaluation.	99% DOX removal after 180 min photocatalytic degradation time.	This study

Conclusıon

The maximum 99% DOX removal efficiency was obtained during photocatalytic degradation process in pharmaceutical industry wastewater, at 150 W UV-vis light irradiation power, after 180 min photocatalytic degradation time, at pH=9.0 and at 25°C, respectively.

The maximum 99% DOX removal efficieny was found with photocatalytic degradation process in pharmaceutical industry wastewater, at 30 mg/l DOX, at 150 W UV-vis light irradiation power, after 180 min photocatalytic degradation time, at pH=9.0 and at 25°C, respectively.

The maximum 99% DOX removal efficieny was measured to 8 mg/l g-C_3N_4/$CoMoO_4$ NCs with photocatalytic degradation process in pharmaceutical industry wastewater, at 30 mg/l DOX, at 150 W UV-vis light irradiation power, after 180 min photocatalytic degradation time, at pH=9.0 and at 25°C, respectively.

The maximum 99% DOX removal efficiency was observed at 6/4wt g-C_3N_4/$CoMoO_4$ NCs mass ratios at 30 mg/l DOX, at 150 W UV-vis light irradiation power, after 180 min photocatalytic degradation time, at pH=9.0 and at 25°C, respectively.

The maximum 99% DOX removal efficiency was obtained in pharmaceutical industry wastewater during photocatalytic degradation process, after 1. recycle time, at 30 mg/l DOX, 8 mg/l g-C_3N_4/$CoMoO_4$ NCs, at 6/4wt g-C_3N_4/$CoMoO_4$ NCs mass ratio, after 180 min photocatalytic degradation time, at pH=9.0 and at 25°C, respectively.

95.33% maximum Microtox (Aliivibrio fischeri) acute toxicity removal yield was found in DOX=30 mg/l after 180 min photocatalytic degradation time and at 60°C, respectively. It was observed an inhibition effect of DOX=45 mg/l to Microtox with Vibrio fischeri after 180 min photocatalytic degradation time and at 60°C. 91.27% maximum Daphnia magna acute toxicity removal was obtained in DOX=30 mg/l after 180 min photocatalytic degradation time and at 60°C, respectively. It was observed an inhibition effect of DOX=45 mg/l to Daphnia magna after 180 min photocatalytic degradation time and at 60°C. DOX concentrations > 30 mg/l decreased the acute toxicity removals by hindering the photocatalytic degradation process. Similarly, a significant contribution of increasing DOX concentrations to acute toxicity removal at 60°C after 180 min photocatalytic degradation time was not observed. Finally, it can be concluded that the toxicity originating from the DOX is not significant and the real acute toxicity throughout photocatalytic degradation process was attributed to the pharmaceutical industry wastewater, to their metabolites and to the photocatalytic degradation process by-products.

As a result, the a novel g-C_3N_4/$CoMoO_4$ NCs photocatalyst during photocatalytic degradation process in pharmaceutical industry wastewater was stable in harsh environments such as acidic, alkaline, saline, and then was still effective process. When the amount of contaminant was increased, the a novel g-C_3N_4/$CoMoO_4$ NCs photocatalys during photocatalytic degradation process performance was still considerable. The synthesis and optimization of g-C_3N_4/$CoMoO_4$ heterostructure photocatalyst provides insights into the effects of preparation conditions on the material's characteristics and performance, as well as the application of the effectively designed photocatalyst in the removal of antibiotics, which can potentially be deployed for purifying wastewater, especially pharmaceutical wastewater. Finally, the combination of a simple, easy operation preparation process, excellent performance and cost effective, makes this a novel g-C_3N_4/$CoMoO_4$ NCs a promising option during photocatalytic degradation process in pharmaceutical industry wastewater treatment.

Acknowledgement

This research study was undertaken in the Environmental Microbiology Laboratories at Dokuz Eylül University Engineering Faculty Environmental Engineering Department, Izmir, Turkey. The authors would like to thank this body for providing financial support.

References

1. Idham MF, Abdullah B, Yusof KM (2017) Effects of two cycle heat treatment on the microstructure and hardness of ductile iron. Pertanika J Sci Technol 25: 99-106.
2. Idham MF, Falyouna O, Eljamal O (2021) Effect of graphene oxide synthesis method on the adsorption performance of pharmaceutical contaminants. Proc Int Exch Innov Conf Eng Sci 7: 232-239.
3. Arenas NE, Melo VM (2018) Producción pecuaria y emergencia de antibiótico resistencia en Colombia. Revisión sistemática Infectio 22: 110-119.
4. Pellerito A, Ameen SM, Micali M, Caruso G (2018) Antimicrobial substances for food packaging products: the current situation. J AOAC Int 101: 942-947.
5. Fridkin S, Baggs J, Fagan R, Magill S, Pollack LA, et al. (2014) Vital signs: improving antibiotic use among hospitalized patients. MMWR-Morb Mortal Wkly Rep 63: 194-200.
6. Tamma PD, Avdic E, Li DX, Dzintars K, Cosgrove SE (2017) Association of adverse events with antibiotic use in hospitalized patients. JAMA Intern Med 177: 1308-1315.
7. Huo TI (2010) The first case of multidrug-resistant NDM−1-harboring Enterobacteriaceae in Taiwan: here comes the superbacteria! J Chin Med Assoc 73: 557-558.
8. Ferri M, Ranucci E, Romagnoli P, Giaccone V (2017) Antimicrobial resistance: A global emerging threat to public health systems. Crit Rev Food Sci 57: 2857-2876.
9. Tan L, Li LY, Ashbolt N, Wang XL, Cui YX, et al. (2018) Arctic antibiotic resistance gene contamination, a result of anthropogenic activities and natural origin. Sci Total Environ 621: 1176-1184.
10. Tong S, Pan J, Lu S, Tang J (2018) Patient compliance with antimicrobial drugs: A Chinese survey. Am J Infect Control 46: E25-E29.
11. Alygizakis NA, Gago-Ferrero P, Borova VL, Pavlidou A, Hatzianestis I, et al. (2016) Occurrence and spatial distribution of 158 pharmaceuticals, drugs of abuse and related metabolites in offshore seawater. Sci Total Environ 541: 1097-1105.
12. Casanova LM, Sobsey MD (2016) Antibiotic-resistant enteric bacteria in environmental waters. Water 8: 561-567.
13. Zhang LH, He YW, Chen M, Gao M, Qiu TL, et al. (2016) Pollution characteristics of antibiotic resistant bacteria from atmospheric environment of animal feeding operations. Huan Jing Ke Xue 37: 4531-4537.
14. Jiménez-Tototzintle M, Ferreira IJ, da Silva Duque S, Guimarães Barrocas PR, Saggioro EM (2018) Removal of contaminants of emerging concern (CECs) and antibiotic resistant bacteria in urban wastewater using UVA/TiO2/H2O2 photocatalysis. Chemosphere 210: 449-457.
15. Kerrigan JF, Sandberg KD, Engstrom DR, LaPara TM, Arnold WA (2018) Small and large-scale distribution of four classes of antibiotics in sediment: association with metals

and antibiotic resistance genes. Environ Sci Process Impacts 20: 1167-1179.

16. Karthikeyan KG, Meyer MT (2006) Occurrence of antibiotics in wastewater treatment facilities in Wisconsin USA. Sci Total Environ 361: 196-207.
17. Dinh QT, Moreau-Guigon E, Labadie P, Alliot F, Teil M-J, et al. (2017) Blanchard, M., Chevreuil, M. Occurrence of antibiotics in rural catchments. Chemosphere 168: 483-490.
18. Dong D, Zhang L, Liu S, Guo Z, Hua X (2016) Antibiotics in water and sediments from Liao River in Jilin Province, China: occurrence, distribution, and risk assessment. Environ Earth Sci 75: 1202.
19. Siedlewicz G, Białk-Bielinska A, Borecka M, Winogradow A, Stepnowski P, et al. (2018) Presence, concentrations and risk assessment of selected antibiotic residues in sediments and near-bottom waters collected from the Polish Coastal Zone in the Southern Baltic Sea—Summary of 3years of studies. Mar Pollut Bull 129: 787-801.
20. Barry S (2019) Dangerously high levels of antibiotics found in world's major rivers, says study, World news global study, Euronews 1: 1-10.
21. Maycock DS, Watts CD (2011) Pharmaceuticals in drinking water. Encycl Environ Heal 472-484.
22. Fekadu S, Alemayehu E, Dewil R, Van der Bruggen B (2019) Pharmaceuticals in freshwater aquatic environments: a comparison of the african and european challenge. Sci Total Environ 654: 324-337.
23. Cui L, Ding X, Wang Y, Shi H, Huang L, et al. (2017) bFacile preparation of Z-scheme WO3/g-C3N4 composite photocatalyst with enhanced photocatalytic performance under visible light. Appl Surf Sci B 391: 202-210.
24. Yang X, Chen Z, Zhao W, Liu C, Qian X, et al. (2021) Recent advances in photodegradation of antibiotic residues in water. Chem Eng J 405: 126806.
25. Akyon B, McLaughlin M, Hernández F, Blotevogel J, Bibby K (2019) Characterization and biological removal of organic compounds from hydraulic fracturing produced water. Environ Sci Process 21: 279-290.
26. Cui G, Guo J, Zhang Y, Zhao Q, Fu S, et al. (2019) Chitosan oligosaccharide derivatives as green corrosion inhibitors for P110 steel in a carbon-dioxide-saturated chloride solution, Carbohydr. Polym 203: 386-395.
27. de Souza Santos LV, Meireles AM, Lange LC (2015) Degradation of antibiotics norfloxacin by fenton, UV and UV/H2O2. J Environ Manag 154: 8-12.
28. Zhong Y, Han L, Yin X, Li H, Fang D, et al. (2018) Three dimensional functionalized carbon/tin(IV) sulfide biofoam for photocatalytical purification of chromium(VI)-containing wastewater. ACS Sustain Chem Eng 6: 10660-10667.
29. Alagha O, Ouerfelli N, Kochkar H, Almessiere MA, Slimani Y, et al. (2021) Kinetic modeling for photo-assisted penicillin G degradation of (Mn0.5Zn0.5)[CdxFe2-x]O4 ($x \leq 0.05$) nanospinel ferrites. Nanomaterials 11: 970-986.
30. Chen Y, Yang J, Zeng L, Zhu M (2022) Recent progress on the removal of antibiotic pollutants using photocatalytic oxidation process. Crit Rev Environ Sci Technol 52: 1401-1448.
31. Sen Gupta PS, Rana MK (2020) Ivermectin, famotidine, and doxycycline: A suggested combinatorial therapeutic for the treatment of COVID-19.ACS Pharmaco Trans Sci 3: 1037-1038.
32. Amini Z, Givianrad MH, Husain SW, Azar PA, Saber-Tehrani M (2020) Cu-S codoping TiO2/SiO2 and TiO2/SiO2/Fe3O4 core-shell nanocomposites as a novel purple LED illumination active photocatalyst for degradation of diclofenac: the effect of different scavenger agents and optimization. Chem Eng Commun 207: 1536-1553.
33. Adams C, Wang Y, Loftin K, Meyer M (2002) Removal of antibiotics from surface and distilled water in conventional water treatment processes. J Environ Eng 128: 253-260.
34. Stackelberg PE, Gibs J, Furlong ET, Meyer MT, Zaugg SD, et al. (2007) Efficiency of conventional drinking-water-treatment processes in removal of pharmaceuticals and other organic compounds. Sci Total Environ 377: 255-272.
35. Garg A, Sangal VK, Bajpai PK (2016) Decolorization and degradation of Reactive Black 5 dye by photocatalysis: Modeling, optimization and kinetic study, Desalin. Water Treat 57: 18003-180015.
36. Bansal P, Verma A, Aggarwal K, Singh A, Gupta S (2016) Investigations on the degradation of an antibiotic Cephalexin using suspended and supported TiO2: Mineralization and durability studies. The Canad J Chem Eng 94: 1269-1276.
37. Rezaei SS, Dehghanifard E, Noorisepehr M, Ghadirinejad K, Kakavandi B, et al. (2019) Efficient clean-up of waters contaminated with diazinon pesticide using photo-decomposition of peroxymonosulfate by ZnO decorated on a magnetic core/shell structure. J Environ Management 250: 109472.
38. Wei Z, Liu J, Shangguan W (2020) A review on photocatalysis in antibiotic wastewater: Pollutant degradation and hydrogen production. Chinese J Catal 41: 1440-1450.
39. Babaei AA, Golshan M, Kakavandi B (2021) A heterogeneous photocatalytic sulfate radical-based oxidation process for efficient degradation of 4-chlorophenol using TiO2 anchored on Fe oxides@ carbon. Process Saf Environ Protection 149: 35-47.
40. Ahammad NA, Zulkifli MA, Ahmad MA, Hameed BH, Mohd Din AT (2021) Desorption of chloramphenicol from ordered mesoporous carbonalginate beads: Effects of operating parameters, and isotherm, kinetics, and regeneration studies. J Environ Chem Eng 9: 105015.
41. Li H, Hu J, Meng Y, Su J, Wang X (2017) An investigation into the rapid removal of tetracycline using multilayered graphene-phase biochar derived from waste chicken feather. Sci Total Environ 603: 39-48.
42. Jiang Q, Zhang Y, Jiang S, Wang Y, Li H, et al. (2020) Graphene-like carbon sheetsupported nZVI for efficient atrazine oxidation degradation by persulfate activation. Chem Eng J 403: 126309.
43. Shirani Z, Song H, Bhatnagar A (2020) Efficient removal of diclofenac and cephalexin from aqueous solution using Anthriscus sylvestris-derived activated biochar. Sci Total Environ 745: 140789.
44. Ahmed MB, Zhou JL, Ngo HH, Guo W (2015) Adsorptive removal of antibiotics from water and wastewater: Progress and challenges. Sci Total Environ 532: 112-126.
45. Khalil AME, Memon FA, Tabish TA, Salmon D, Zhang S, et al. (2020) Nanostructured porous graphene for efficient removal of emerging contaminants (pharmaceuticals) from water. Chem Eng J 398: 125440.
46. Avcu T, Üner O, Geçgel Ü (2021) Adsorptive removal of diclofenac sodium from aqueous solution onto sycamore ball activated carbon – isotherms, kinetics, and thermodynamic study. Surfaces and Interfaces 24: 101097.
47. Ji Y, Zhang C, Zhang XJ, Xie PF, Wu C, et al. (2022) A high adsorption capacity bamboo biochar for CO2 capture for low temperature heat utilization. Sep Purif Technol 293: 121131.
48. Shahnaz T, Vishnu Priyan V, Pandian S, Narayanasamy S (2021) Use of nanocellulose extracted from grass for adsorption abatement of ciprofloxacin and diclofenac removal with phyto, and fish toxicity studies. Environ Pollut 268: 115494.

49. Wang Z, Song L, Wang Y, Zhang XF, Yao J (2021) Construction of a hybrid graphene oxide/nanofibrillated cellulose aerogel used for the efficient removal of methylene blue and tetracycline. J Phys Chem Solids 150: 109839.
50. Cui G, Guo J, Zhang Y, Zhao Q, Fu S, et al. (2019) Chitosan oligosaccharide derivatives as green corrosion inhibitors for P110 steel in a carbon-dioxide-saturated chloride solution, Carbohydr. Polym 203: 386-395.
51. Phasupha W, Praphairaksit N, Imyim A (2019) Removal of ibuprofen, diclofenac, and naproxen from water using chitosan-modified waste tire crumb rubber. J Mol Liq 294: 111554.
52. ALOthman ZA, Badjah AY, Alharbi OML, Ali I (2020) Synthesis of chitosan composite iron nanoparticles for removal of diclofenac sodium drug residue in water. Int J Biol Macromol 159: 870-876.
53. Yu F, Sun S, Han S, Zheng J, Ma J (2016) Adsorption removal of ciprofloxacin by multi-walled carbon nanotubes with different oxygen contents from aqueous solutions. Chem Eng J 285: 588-595.
54. Zhao H, Liu X, Cao Z, Zhan Y, Shi X, et al. (2016) Adsorption behavior and mechanism of chloramphenicols, sulfonamides, and nonantibiotic pharmaceuticals on multi-walled carbon nanotubes. J Hazard Mater 310: 235-245.
55. Bellamkonda S, Thangavel N, Hafeez HY, Neppolian B, Ranga Rao G (2019) Highly active and stable multi-walled carbon nanotubes-graphene-TiO2 nanohybrid: An efficient non-noble metal photocatalyst for water splitting. Catal Today 321-322: 120-127.
56. Rigueto CVT, Rosseto M, Nazari MT, Ostwald BEP, Alessandretti I, et al. (2021) Adsorption of diclofenac sodium by composite beads prepared from tannery wastesderived gelatin and carbon nanotubes. J Environ Chem Eng 9: 105030.
57. Ahmed MB, Zhou JL, Ngo HH, Guo W, Johir MAH, et al. (2017) Nano-Fe0 immobilized onto functionalized biochar gaining excellent stability during sorption and reduction of chloramphenicol via transforming to reusable magnetic composite. Chem Eng J 322: 571-581.
58. Yu H, Wang D, Zhao B, Lu Y, Wang X, et al. (2020) Enhanced photocatalytic degradation of tetracycline under visible light by using a ternary photocatalyst of Ag3PO4/AgBr/g-C3N4 with dual Z-scheme heterojunction, Separ. Purif Tech 237: 116365.
59. Nguyen LT, Nguyen HT, Pham TD, Tran TD, Chu HT, et al. (2020) UV–visible light driven photocatalytic degradation of ciprofloxacin by N, S co-doped TiO2: the effect of operational parameters. Topics in Catalysis 63: 985-995.
60. Nguyen CH, Tran ML, Van Tran TT, Juang RS (2021) Efficient removal of antibiotic oxytetracycline from water by Fenton-like reactions using reduced graphene oxide-supported bimetallic Pd/nZVI nanocomposites. J Taiwan Inst Chem Eng 119: 80-89.
61. Falyouna O, Idham MF, Maamoun I, Bensaida K, Ashik UPM, et al. (2022) Promotion of ciprofloxacin adsorption from contaminated solutions by oxalate modified nanoscale zerovalent iron particles. J Mol Liq 359: 119323.
62. Falyouna O, Maamoun I, Bensaida K, Tahara A, Sugihara Y, et al. (2022) Encapsulation of iron nanoparticles with magnesium hydroxide shell for remarkable removal of ciprofloxacin from contaminated water. J Colloid Interface Sci 605: 813-827.
63. Mokhati A, Benturki O, Bernardo M, Kecira Z, Matos I, et al. (2021) Nanoporous carbons prepared from argan nutshells as potential removal agents of diclofenac and paroxetine. J Mol Liq 326: 115368.
64. Shan D, Deng S, Li J, Wang H, He C, et al. (2017) Preparation of porous graphene oxide by chemically intercalating a rigid molecule for enhanced removal of typical pharmaceuticals. Carbon N Y 119: 101-109.
65. Khalil AME, Memon FA, Tabish TA, Salmon D, Zhang S, et al. (2020) Nanostructured porous graphene for efficient removal of emerging contaminants (pharmaceuticals) from water. Chem Eng J 398: 125440.
66. Görmez F, Görmez Ö, Gözmen B, Kalderis D (2019) Degradation of chloramphenicol and metronidazole by electro-fenton process using graphene oxideFe3O4 as heterogeneous catalyst. J Environ Chem Eng 7: 102990.
67. Qiao D, Li Z, Duan J, He X (2020) Adsorption and photocatalytic degradation mechanism of magnetic graphene oxide/ZnO nanocomposites for tetracycline contaminants. Chem Eng J 400: 125952.
68. Yadav S, Asthana A, Singh AK, Chakraborty R, Vidya SS, et al. (2021) Methionine-functionalized graphene oxide/sodium alginate bio-polymer nanocomposite hydrogel beads: synthesis, ısotherm and kinetic studies for an adsorptive removal of fluoroquinolone antibiotics. Nanomaterials 11: 568-593.
69. Li Y, Gutiérrez Moreno JJ, Song Z, Liu D, Wang M, et al. (2022) Controlled synthesis of perforated oxide nanosheets with high density nanopores showing superior water purification performance. ACS Appl Mater Interfaces 14: 18513-18524.
70. Bao J, Zhu Y, Yuan S, Wang F, Tang H, et al. (2018) Adsorption of tetracycline with reduced graphene oxide decorated with MnFe2O4 nanoparticles. Nanoscale Res Lett 13: 396-403.
71. Tang H, Li W, Jiang H, Lin R, Wang Z, et al. (2019) ZIF-8-derived hollow carbon for efficient adsorption of antibiotics. Nanomaterials 9: 117.
72. Tang H, Li W, Jiang H, Lin R, Wang Z, et al. (2019) ZIF-8-derived hollow carbon for efficient adsorption of antibiotics. Nanomaterials 9: 117.
73. Masoudi F, Kamranifar M, Safari F, Naghizadeh A (2019) Mechanism, kinetics and thermodynamic of Penicillin G antibiotic removal by silica nanoparticles from simulated hospital wastewater. Desalination Water Treat 169: 333-341.
74. Zeidman AB, Rodriguez-Narvaez OM, Moon J, Bandala ER (2020) Removal of antibiotics in aqueous phase using silica-based ımmobilized nanomaterials: a review. Environ Technol Innov 20: 101030.
75. Sturini M, Puscalau C, Guerra G, Maraschi F, Bruni G, et al. (2021) Combined layer-by-layer/hydrothermal synthesis of Fe3O4@MIL-100(Fe) for ofloxacin adsorption from environmental waters. Nanomaterials 11: 3275.
76. Li Y, Gutiérrez Moreno JJ, Song Z, Liu D, Wang M, et al. (2022) Controlled synthesis of perforated oxide nanosheets with high density nanopores showing superior water purification performance. ACS Appl Mater Interfaces 14: 18513-18524.
77. Dehghan A, Mohammadi AA, Yousefi M, Najafpoor AA, Shams M, et al. (2019) Enhanced kinetic removal of ciprofloxacin onto metal-organic frameworks by sonication, process optimization and metal leaching study. Nanomaterials 9: 1422-1438.
78. Sun T, Fan R, Zhang J, Qin M, Chen W, et al. (2021) Stimuli-Responsive metal–organic framework on a metal–organic framework heterostructure for efficient antibiotic detection and anticounterfeiting. ACS Appl Mater Interfaces 13: 35689-35699.

79. Luo B, Xu D, Li D, Wu G, Wu M, et al. (2015) Fabrication of a Ag/Bi3TaO7 plasmonic photocatalyst with enhanced photocatalytic activity for degradation of tetracycline. ACS Appl Mater Interfaces 7: 17061-17069.
80. Lu Y, Chu Y, Zheng W, Huo M, Huo H, et al. (2019) Significant tetracycline hydrochloride degradation and electricity generation in a visible-light-driven dual photoelectrode photocatalytic fuel cell using BiVO4/TiO2 NT photoanode and Cu2O/TiO2 NT photocathode. Electrochim Acta 320: 134617.
81. Yu H, Wang D, Zhao B, Lu Y, Wang X, et al. (2020) Enhanced photocatalytic degradation of tetracycline under visible light by using a ternary photocatalyst of Ag3PO4/AgBr/g-C3N4 with dual Z-scheme heterojunction, Separ. Purif Tech 237: 116365.
82. Chen Y, Yang J, Zeng L, Zhu M (2022) Recent progress on the removal of antibiotic pollutants using photocatalytic oxidation process. Crit Rev Environ Sci Technol 52: 1401-1448.
83. Fu J, Yu J, Jiang C, Cheng B (2018) g-C3N4-based heterostructured photocatalysts. Adv Energy Mater 8: 1701503.
84. Ren Y, Zeng D, Ong WJ (2019) Interfacial engineering of graphitic carbon nitride (g-C3N4)-based metal sulfide heterojunction photocatalysts for energy conversion: A review. Chin J Catal 40: 289-319.
85. Hao Q, Chen T, Wang R, Feng J, Chen D, et al. (2018) A separation-free polyacrylamide/bentonite/graphitic carbon nitride hydrogel with excellent performance in water treatment. J Clean Prod 197: 1222-1230.
86. Hao X, Zhou J, Cui Z, Wang Y, Wang Y, et al. (2018) Zn-vacancy mediated electron-hole separation in ZnS/g-C3N4 heterojunction for efficient visible-light photocatalytic hydrogen production. Appl Catal B 229: 41-51.
87. Mestre AS, Carvalho AP (2019) Photocatalytic degradation of pharmaceuticals carbamazepine, diclofenac, and sulfamethoxazole by semiconductor and carbon materials: a review. Molecules 24: 3702.
88. Low J, Jiang C, Chen B, Wageh S, Al-Ghamdi AA, et al. (2017) A review of direct Z-scheme photocatalysts. Small Methods 1: 1700080.
89. Chen Y, Fan ZX, Zhang ZC, Niu WX, Li CL, et al. (2018) Two-dimensional metal nanomaterials: synthesis, properties, and applications. Chem Rev 118: 6409-6455.
90. Xu Q, Zhang L, Yu J, Wageh S, Al-Ghamdi AA, et al. (2018) Direct Z-scheme photocatalysts: Principles, synthesis, and applications. Mater Today 21: 1042-1063.
91. Huang D, Chen S, Zeng G, Gong X, Zhou CY, et al. (2019) Artificial Z-scheme photocatalytic system: What have been done and where to go? Coord Chem Rev 385: 44-80.
92. Lu ZY, Ma YL, Zhang JT, Fan NS, Huang BC, et al. (2020) A critical review of antibiotic removal strategies: Performance and mechanisms. J Water Process Eng 38: 101681
93. Yu W, Xu D, Peng T (2015) Enhanced photocatalytic activity of g-C3N4 for selective CO2 reduction to CH3OH via facile coupling of ZnO: a direct Z-scheme mechanism J Mater Chem A 3: 19936-19947.
94. Liu D, Zhang M, Xie W, Sun L, Chen Y, et al. (2017) Porous BN/TiO2 hybrid nanosheets as highly efficient visible-light-driven photocatalysts. Appl Catal B-Environ 207: 72-78.
95. Wang J, Hao J, Liu D, Qin S, Chen C, et al. (2017) Flower stamen-like porous boron carbon nitride nanoscrolls for water cleaning. Nanoscale 9: 9787-9791.
96. Liu X, Pang F, He M, Ge J (2017) Confined reaction inside nanotubes: New approach to mesoporous g-C3N4 photocatalysts. Nano Res 10: 3638-3647.
97. Cui L, Ding X, Wang Y, Shi H, Huang L, et al. (2017) bFacile preparation of Z-scheme WO3/g-C3N4 composite photocatalyst with enhanced photocatalytic performance under visible light. Appl Surf Sci B 391: 202-210.
98. Gebreslassie G, Bharali P, Chandra U, Sergawie A, Boruah PK, et al. (2019) Novel g-C3N4/graphene/NiFe2O4 nanocomposites as magnetically separable visible light driven photocatalysts. J Photochem Photobiol A 382: 111960.
99. Gebreslassie G, Bharali P, Chandra U, Sergawie A, Boruah PK, et al. (2019) Hydrothermal synthesis of g-C3N4/NiFe2O4 nanocomposite and its enhanced photocatalytic activity. Appl Organomet Chem 33: e5002.
100. Wu J, Hu J, Qian H, Li J, Yang R, et al. (2022) NiCo/ZnO/g-C3N4 Z-scheme heterojunction nanoparticles with enhanced photocatalytic degradation oxytetracycline. Diamond Relat Mater 121: 108738.
101. Qu Z, Jing Z, Chen X, Wang Z, Ren H, et al. (2023) Preparation and photocatalytic performance study of dual Z-scheme Bi2Zr2O7/g-C3N4/Ag3PO4 for removal of antibiotics by visible-light. J Environ Sci 125: 349-361.
102. Zhao H, Yu H, Quan X, Chen S, Zhang Y, et al. (2014) Fabrication of atomic single layer graphiticC3N4 and its high performance of photocatalytic disinfection under visible light irradiation. Appl Catal B 152: 46-50.
103. Mamba G, Mishra AK (2016) Graphitic carbon nitride (gC3N4) nanocomposites: A new and exciting generation of visible light driven photocatalysts for environmental pollution remediation. Appl Catal B 198: 347-377.
104. Darkwah WK, Ao Y (2018) Mini review on the structure and properties (photocatalysis), and preparation techniques of graphitic carbon nitride nano-based particle, and its applications. Nanoscale Res Lett 13: 388
105. Oh WD, Chang VWC, Hu ZT, Goei R, Lim TT (2017) Enhancing the catalytic activity of g-C3N4 through Me doping (Me = Cu, Co and Fe) for selective sulfathiazole degradation via redox-based advanced oxidation process. Chem Eng J 323: 260-269.
106. Wang ZT, Xu JL, Zhou H, Zhang X (2019) Facile synthesis of Zn(II)-doped g-C3N4 and their enhanced photocatalytic activity under visible light irradiation. Rare Met 38: 459-467.
107. Dai Y, Gu Y, Bu Y (2020) Modulation of the photocatalytic performance of g-C3N4 by two-sites co-doping using variable valence metal. Appl Surf Sci 500: 144036.
108. Ye L, Liu J, Jiang Z, Peng T, Zan L (2013) Facets coupling of BiOBr-g-C3N4 composite photocatalyst for enhanced visible-light-driven photocatalytic activity. Appl Catal B 142: 1-7.
109. Tian N, Huang H, He Y, Guo Y, Zhang T, et al. (2015) Mediator-free direct Z-scheme photocatalytic system: BiVO4/g-C3N4 organic–inorganic hybrid photocatalyst with highly efficient visible-light-induced photocatalytic activity. Dalton Trans 44: 4297-4307.
110. Nithya R, Ayyappan S (2020) Novel exfoliated graphiticC3N4 hybridised ZnBi2O4 (g-C3N4/ZnBi2O4) nanorods for catalytic reduction of 4-Nitrophenol and its antibacterial activity. J Photochem Photobiol Chem 398: 112591.
111. Tian N, Huang H, Wang S, Zhang T, Du X, et al. (2020) Facet-charge-induced coupling dependent interfacial photocharge separation: A case of BiOI/g-C3N4 p-n junction. Appl Catal B 267: 118697.
112. Liu S, Chen F, Li S, Peng X, Xiong Y (2017) Enhanced photocatalytic conversion of greenhouse gas CO2 into solar fuels over g-C3N4 nanotubes with decorated transparent ZIF-8 nanoclusters. Appl Catal B 211: 1-10.
113. Dai Y, Gu Y, Bu Y (2020) Modulation of the photocatalytic performance of g-C3N4 by two-sites co-doping using variable

valence metal. Appl Surf Sci 500: 144036.
114. Veerasubramani GK, Krishnamoorthy K, Radhakrishnan S, Kim NJ, Kim SJ (2017) Synthesis, characterization, and electrochemical properties of CoMoO4 nanostructures. Int J Hydrogen Energy 39: 5186-5193.
115. Umapathy V, Neeraja P (2016) Sol–gel synthesis and characterizations of CoMoO4 nanoparticles: an efficient photocatalytic degradation of 4-chlorophenol. J Nanosci Nanotechnol 16: 2960-2966.
116. Zagorac D, Schön JC, Rosić M, Zagorac J, Jordanov D, et al. (2017) Theoretical and experimental study of structural phases in CoMoO4. Cryst Res Technol 52: 1700069.
117. Feizpoor S, Habibi-Yangjeh A, Yubuta K, Vadivel S (2019) Fabrication of TiO2/CoMoO4/PANI nanocomposites with enhanced photocatalytic performances for removal of organic and inorganic pollutants under visible light. Mater Chem Phys 224: 10-21.
118. Gao Z, Yang H, Cao Y, Wu Q, Kang L, et al (2019) Complete mineralization of a humic acid by SO4 generated on CoMoO4/gC3N4 under visible-light irradiation, Nanotechnology 30: 255704.
119. Adabavazeh H, Saljooqi A, Shamspur T, Mostafavi A (2021) Synthesis of polyaniline decorated with ZnO and CoMoO4 nanoparticles for enhanced photocatalytic degradation of imidacloprid pesticide under visible light. Polyhedron 198: 115058.
120. Habibi-Yangjeh A, Mousavi M, Nakata K (2019) Boosting visible-light photocatalytic performance of g-C3N4/ Fe3O4 anchored with CoMoO4 nanoparticles: Novel magnetically recoverable photocatalysts. J Photochem Photobiol Chem 368: 120-136.
121. Zhang W, Mohamed AR, Ong WJZ (2020) scheme photocatalytic systems for carbon dioxide reduction: where are we now? Angew Chem Int Ed 59: 22894-22915.
122. Baird RB, Eaton AD, Rice EW (2017) Standard Methods for the Examination of Water and Wastewater. 23rd. Edition, Rice, EW (editors) American Public Health Association (APHA), American Water Works Association (AWWA), Water Environment Federation (WEF). American Public Health Association 800 I Street, NW Washington.
123. Olthof M, Eckenfelder WW (1976) Coagulation of textile wastewater. Textile, Chemistry and Colorists 8: 18-22.
124. Eckenfelder WW (1989) Industrial Water Pollution Control (2nd ed) Signapore: McGraw-Hill Inc.
125. Lange B (1994) LUMISmini, Operating Manual. Düsseldorf, Germany: Dr Bruno LANGE.
126. Lange B (2010) Vibrio fischeri -Microtox LCK 491 kit. Germany: Dr LANGE.
127. Lange B (1996) LUMIXmini type luminometer. Dusseldorf: Dr LANGE Company.
128. Zar JH (1984) Biostatistical analysis, Prentice-Hall, Englewood Cliffs.
129. Statgraphics Centurion XV, sofware, StatPoint Inc, Statgraphics Centurion XV, Herndon, VA, USA, 2005.
130. Liu W, Li Z, Kang Q, Wen L (2021) Efficient photocatalytic degradation of doxycycline by coupling α-Bi2O3/g-C3N4 composite and H2O2 under visible light. Environmental Research 197: 110925.
131. Mohammadi A, Pourmoslemi S (2017) Enhanced photocatalytic degradation of doxycycline using a magnetic polymer-ZnO composite. Water Science Technology 3: 791-801.
132. Romanovska NI, Manoryk PA, Selyshchev OV, Ermokhina NI, Yaremov PS, et al. (2020) Effect of the modification of TiO2 with thiourea on its photocatalytic activity in doxycycline degradation. Theoretical and Experimental Chemistry 56: 183-191.
133. Liu W, Zhou J, Zhou J (2019) Facile fabrication of multi-walled carbon nanotubes (MWCNTs)/α-Bi2O3 nanosheets composite with enhanced photocatalytic activity for doxycycline degradation under visible light irradiation. Journal of Materials Science 54: 3294-3308.
134. Gao J, Gao Y, Sui Z, Dong Z, Wang S, et al. (2018) Hydrothermal synthesis of BiOBr/FeWO4 composite photocatalysts and their photocatalytic degradation of doxycycline. Journal of Alloys Compounds 732: 43-51.
135. Tien NTC, Nhut CH, Thuy VTT, Huyen TTB, Hien LPT, et al. (2022) Enhancement in photocatalytic efficiency of commercial TiO2 nanoparticles by calcination: A case of doxycycline removal, Bulletin of Chemical Reaction Engineering & Catalysis 17: 486-496.